8

Mathematical Models for Multiphase Flow

Up to now, we have only considered flow of a single fluid phase. For most applications of reservoir simulation, however, one is interested in modeling how one fluid phase displaces one or more other fluid phases. In hydrocarbon recovery, typical examples are water or gas flooding, in which injected water or gas displaces the resident hydrocarbon phase(s). Likewise, in geological carbon sequestration, the injected CO_2 forms a supercritical fluid phase that displaces the resident brine. In both cases, more than one phase will flow simultaneously throughout the porous medium when viewed from the scale of a representative elementary volume, even if the fluids are immiscible and do not mix on the microscale.

To model such flows, we introduce three new physical properties of multiphase models (saturation, relative permeability, and capillary pressure) and discuss how one can use these to extend Darcy's law to multiphase flow and combine it with conservation of mass for each fluid phase to develop models describing multiphase displacements. The resulting system of partial differential equations is parabolic in the general case, but has a mixed elliptic-hyperbolic mathematical character. Fluid pressures tend to behave as following a near-elliptic equation, whereas the transport of fluid phases has a strong hyperbolic character. It is therefore common to use a so-called fractional-flow formulation to write the flow equations as a coupled system consisting of a pressure equation describing the evolution of one of the fluid pressures and (a system of) saturation equation(s) that describes the transport of fluid phases. The mixed elliptic-hyperbolic nature is particularly evident in the case of immiscible, incompressible flow. In this case, the pressure equation simplifies to a Poisson equation of the same form we have studied in previous chapters.

This chapter describes the new physical effects that appear in multiphase flow and discusses general multiphase models in some detail. We also derive the fractional-flow formulation in the special case of immiscible flow and analyze the mathematical character of the system in certain limiting cases. Chapter 9 introduces various methods for solving hyperbolic transport equation and reviews some of the supporting theory. Then, in Chapter 10, we focus entirely on the incompressible case and show how we can easily reuse the elliptic solvers developed in the previous chapters and combine them with a set of simple first-order transport solvers that are implemented in the `incomp` module of MRST. To simplify the discussion, this and the next two chapters will mainly focus on two-phase,

https://doi.org/10.1017/9781108591416.012 Published online by Cambridge University Press

immiscible systems, but the most crucial equations will be stated and developed for the general multiphase case. In Chapters 11 and 12, we return to the general case and discuss the compressible models and numerical methods that are used for three-phase flow in most contemporary commercial simulators.

8.1 New Physical Properties and Phenomena

As we have seen previously, a Darcy-type continuum description of a reservoir fluid system means that any physical quantity defined at a point $\vec{x}$ represents an average over a representative elementary volume (REV). Let us consider a system with two or more fluid phases that are *immiscible* so that no mass transfer takes place among the phases. This means that the fluid phases will not mix and form a solution on the microscale but rather stay as separate volumes or layers separated by a curved meniscus as illustrated in Figure 8.1. Nevertheless, when considering the flow averaged over a REV, the fluid phases will generally not be separated by a sharp interface, and two or more phases may occupy the same point in the continuum description. In this section, we introduce the new fundamental concepts necessary to understand multiphase flow and formulate continuum models that describe the simultaneous flow of two or more fluid phases taking place at the same point in a reservoir. Unless stated otherwise, the two fluids are assumed to be oil and water when we discuss two-phase systems.

8.1.1 Saturation

Saturation S_α is defined as the fraction of the pore volume occupied by phase α. In the single-phase models discussed in previous chapters, we assumed that the void space between the solid particles that make up the porous medium was completely filled by fluid. Similarly, for multiphase models we assume that the void space is completely filled with one or more fluid phases, so that

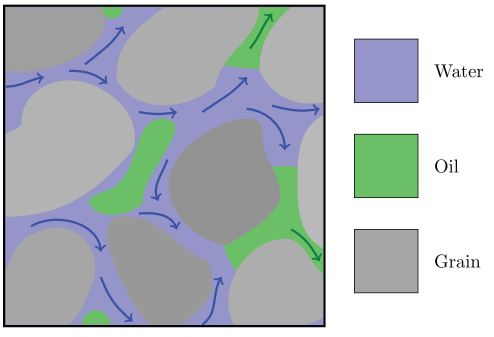

Figure 8.1 Averaging of a multiphase flow over a representative elementary volume (REV) to obtain a Darcy-scale continuum model.

https://doi.org/10.1017/9781108591416.012 Published online by Cambridge University Press

$$\sum_{\alpha} S_{\alpha} = 1. \tag{8.1}$$

In reservoir simulation, it is most common to consider three phases: an aqueous phase (w), an oleic phase (o), and a gaseous (g) phase. Each saturation can vary from 0, which means that the phase is not present at all at this point in space, to 1, which means that the phase completely fills the local pore volume. In most practical cases, however, the range of variability is smaller.

Consider a rock originally deposited in an aqueous environment. During deposition, the pores between rock particles are completely filled with water. Later, as hydrocarbons start to migrate into what is to become our reservoir, the resident water will be displaced and the saturation gradually reduced to some small value, typically 5–40%, at which the water can no longer flow and exists as small drops trapped between mineral particles or encapsulated by the invading hydrocarbon phases. The saturation at which water goes from being mobile (funicular state) to being immobile (pendular state) is called the *irreducible water saturation* and is usually denoted S_{wir} or S_{wr}. The irreducible water saturation is determined by the topology of the pore space and the water's affinity to wet the mineral particles relative to that of the invading hydrocarbons; this affinity is determined by the chemical composition of the fluids and the mineral particles.

Petroleum literature also talks of the *connate water saturation*, usually denoted S_{wc}, which is the water saturation that exists upon discovery of the reservoir. The quantities S_{wir} and S_{wc} may or may not coincide, but should not be confused. Sometimes, one also sees the notation S_{wi}, which may refer to any of the two. If water is later injected to displace the oil, it is generally not possible to flush out all the oil and parts of the pore space will be occupied by isolated oil droplets, as illustrated in Figure 8.1. The corresponding *residual oil saturation* is denoted as S_{or}. In most systems, the water has a stronger affinity for the rock, which means that S_{or} is usually higher than S_{wr} and S_{wc}: typically they are in the range 10–50%.

In many models, each phase may also contain one or more *components*. These may be unique hydrocarbon species like methane, ethane, propane, etc., or other chemical species like polymers, salts, surfactants, tracers, etc. Since the number of hydrocarbon components can be quite large, it is common to group components into *pseudo-components*. Because of the varying and extreme conditions in a reservoir, the composition of the different phases can change throughout a simulation and may sometimes be difficult to determine uniquely. We therefore need to describe this composition. There are several ways to do this. Herein, we use the mass fraction of component ℓ in phase α, denoted by c_{α}^{ℓ} and defined as

$$c_{\alpha}^{\ell} = \frac{\rho_{\alpha}^{\ell}}{\rho_{\alpha}} \tag{8.2}$$

where ρ_{α} denotes the bulk density of phase α and ρ_{α}^{ℓ} the effective density of component ℓ in phase α. In each phase, the mass fractions should add up to unity, so that for M different components in a system consisting of an aqueous, a gaseous, and an oleic phase, we have:

https://doi.org/10.1017/9781108591416.012 Published online by Cambridge University Press

$$\sum_{\ell=1}^{M} c_w^\ell = \sum_{\ell=1}^{M} c_g^\ell = \sum_{\ell=1}^{M} c_o^\ell = 1. \tag{8.3}$$

We will return to models having three phases and more than one component per phase in Chapter 11. For now, however, we assume that our system consists of two immiscible phases.

8.1.2 Wettability

At the microscale, which is significantly larger than the molecular scale, immiscible fluid phases are separated by well-defined, infinitely thin interfaces. Because cohesion forces between molecules are different on opposite sides, each interface has an associated *surface tension* (or surface energy), which measures the forces the interface must overcome to change its shape. In the absence of external forces, minimization of surface energy will cause the interface of a droplet of one phase contained within another phase to assume a spherical shape. The interface tension will keep the fluids apart, regardless of the size of the droplet.

The microscale flow of our oil–water system is strongly affected by how the phases attach to the interface of the solid rock. The ability of a liquid phase to maintain contact with a solid surface is called *wettability* and is determined by intermolecular interactions when the liquid and solid are brought together. Adhesive forces between different molecules in the liquid phase and the solid rock will cause liquid droplets to spread across the mineral surface. Likewise, cohesive forces between similar molecules within the liquid phases will cause the droplets to avoid contact with the surface and ball up. When two fluid phases are present in the same pore space, one phase will be more attracted to the mineral particles than the other phase. We refer to the preferential phase as the *wetting phase*, while the other is called the *non-wetting phase*. The balance of the adhesive and cohesive forces determines the *contact angle* θ shown in Figure 8.2, which is a measure of the wettability of a system that can be related to the interface energies by Young's equation:

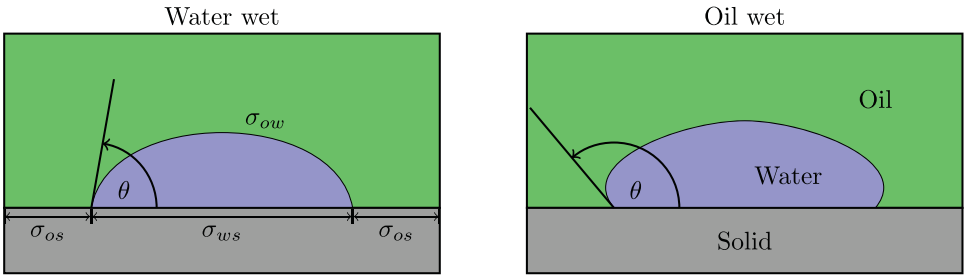

Figure 8.2 Contact angle θ and surface tension σ for two different oil–water systems. In water-wet systems, $0 \leq \theta < 90^\circ$, whereas $90^\circ < 180^\circ$ in oil-wet systems.

https://doi.org/10.1017/9781108591416.012 Published online by Cambridge University Press

$$\sigma_{ow} \cos\theta = \sigma_{os} - \sigma_{ws}. \tag{8.4}$$

Here, σ_{ow} is the interface energy of the oil–water interface and σ_{os} and σ_{ws} are the energies of the oil–solid and water–solid interfaces, respectively. Hydrophilic or water-wet porous media, in which the water shows a greater affinity than oil to stick to the rock surface, are more widespread in nature than hydrophobic or oil-wet media. This explains why S_{or} usually is larger than S_{wr}. In a perfectly water-wet system, $\theta = 0$ so that water spreads evenly over the whole surface of the mineral grains. Likewise, in a perfectly oil-wet system, $\theta = 180^\circ$, so that water forms spherical droplets at the solid surface.

8.1.3 Capillary Pressure

Because of the surface tension, the equilibrium pressure in two phases separated by a curved interface will generally be different. The difference in phase pressures is called the *capillary pressure*,

$$p_c = p_n - p_w, \tag{8.5}$$

and is always positive because the pressure in the non-wetting fluid is higher than the pressure in the wetting fluid. For a water-wet reservoir, the capillary pressure is therefore defined as $p_{cow} = p_o - p_w$, whereas one usually defines $p_{cog} = p_g - p_o$ in an oil–gas system where oil is the wetting phase.

The action of capillary pressures can cause liquids to move in narrow spaces, devoid of or in opposition to other external forces such as gravity. To illustrate this, we consider a thin tube immersed in a wetting and a non-wetting fluid, as shown in Figure 8.3. For the wetting fluid, adhesive forces between the solid tube and the liquid will form a concave meniscus and pull the liquid upward against the gravity force. It is exactly the same effect that causes water to be drawn up into a piece of cloth or paper dipped into water. In the non-wetting case, the intermolecular cohesion forces within the liquid exceed the adhesion forces between the liquid and the solid so that a convex meniscus is formed and drawn downwards relative to the liquid level outside of the tube. At equilibrium inside the capillary

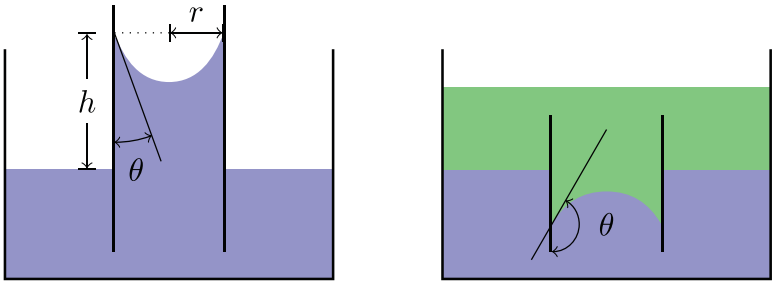

Figure 8.3 Capillary tubes for a wetting liquid and air (left) and a wetting and a non-wetting liquid (right). (The width of the capillary tube is exaggerated.)

https://doi.org/10.1017/9781108591416.012 Published online by Cambridge University Press

tube, the upward and downward forces must balance each other. The force acting upward equals

$$2\pi r(\sigma_{as} - \sigma_{ls}) = 2\pi r\,\sigma\cos\theta,$$

where subscripts a and l refer to air and liquid, respectively. The capillary pressure is defined as force per unit area, or in other words,

$$p_c = \frac{2\pi r\,\sigma\cos\theta}{\pi r^2}. = \frac{2\sigma\cos\theta}{r} \tag{8.6}$$

The force acting downward can be deducted from Archimedes' principle as $\pi r^2 gh(\rho_l - \rho_a)$. By equating this with the action of the capillary pressure, we obtain

$$p_c = \frac{\pi r^2\, gh(\rho_l - \rho_a)}{\pi r^2} = \Delta\rho gh. \tag{8.7}$$

Void space inside a reservoir contains a large number of narrow pore throats that can be thought of as a bundle of nonconnecting capillary tubes of different radius. As we can see from the formulas developed thus far, the capillary pressure increases with decreasing tube radius for a fixed interface-energy difference between two immiscible fluids. Because the pore size is usually so small, capillary pressure will play a major role in establishing the fluid distribution inside the reservoir. To see this, consider a hydrocarbon phase migrating upward by buoyancy forces into a porous rock filled with water. If the hydrocarbon phase is to enter void space in the rock, its buoyancy force must exceed a certain minimum capillary pressure. The capillary pressure that is required to force the first droplet of oil into the rock is called the *entry pressure*. If we consider the rock as a complex assortment of capillary tubes, the first droplet will enter the widest tube, which according to (8.6) has the lowest capillary pressure. As the pressure difference between the buoyant oil and the resident water increases, oil will be able to enter increasingly smaller pore throats and hence reduce the water saturation. This means that there will be a relation between saturation and capillary pressure,

$$p_{cnw} = p_n - p_w = P_c(S_w), \tag{8.8}$$

as illustrated in Figure 8.4. The slope of the curve is determined by the variability of the pore sizes. If all pores are of similar size, they will all be invaded quickly once we exceed the entry pressure and the curve will be relatively flat so that saturation decays rapidly with increasing capillary pressure. If the pores vary a lot in size, the decrease in saturation with increasing capillary pressure will be more gradual. As for the vertical distribution of fluids, we see that once the fluids have reached a hydrostatic equilibrium, the difference in densities between water and oil dictates the difference in phase pressures and hence oil saturation increases in the upward direction, which is also illustrated in the figure.

https://doi.org/10.1017/9781108591416.012 Published online by Cambridge University Press

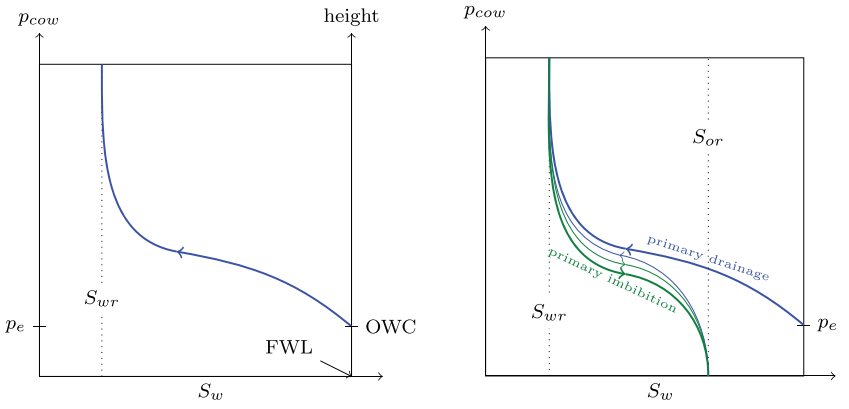

Figure 8.4 The left plot shows a capillary pressure curve giving the relation between capillary pressure p_{cow} and water saturation S_w. In addition, we have included how the capillary pressure and water saturation relate to the height above the free water level (FWL) for a system in hydrostatic equilibrium. Notice that the entry pressure p_e occurs at the oil–water contact (OWC), which is found above the FWL for systems with nonzero entry pressures. The right plot shows hysteretic behavior for repeated drainage and imbibition displacements.

Hysteresis, Drainage, and Imbibition

The argument earlier in this section was for the case of an invading non-wetting fluid displacing a wetting fluid. This type of displacement is called *drainage* to signify that the saturation of the wetting phase is decreasing in this type of displacement. The opposite case, called *imbibition*, occurs when a wetting fluid displaces a non-wetting fluid. As an example, let us assume that we inject water to flush out the oil in a pristine reservoir, in which the amount of connate water equals the irreducible water saturation. During this displacement, the water saturation will gradually increase as more water is injected. Hence, the oil saturation decreases until we reach the residual oil saturation, at which there is only *immobile oil* left. The displacement will generally not follow the same capillary curve as the primary drainage curve, as shown in the right plot in Figure 8.4. Likewise, if another drainage displacement takes place, starting from S_{or} or a larger oil saturation, this process will generally not follow the imbibition curve. The result is an example of what is called *hysteresis*, in which the behavior of a system depends both on the current state and its previous history. The hysteretic behavior can be explained by pore-scale trapping of oil droplets, by variations in the wetting angle between advancing and receding fluid at the solid interface, and by the fact that whereas the drainage process is controlled by the size of the widest non-invaded pore throat, the imbibition process is controlled by the size of the narrowest non-invaded pore.

As we can see from Figure 8.4, a relatively large fraction of the oil will be left behind in an immobile state after waterflooding. Several methods for enhanced oil recovery have been developed to mobilize this immobile oil, e.g., by injecting another fluid (e.g., CO_2 or gas) that mixes with immobile oil droplets so that a larger fraction of the oil can be washed

https://doi.org/10.1017/9781108591416.012 Published online by Cambridge University Press

out along with the invading fluid. In chemical and microbial methods, one adds chemical substances or small microorganisms to the injected fluids that alter the wetting properties inside the pores. Simulating these processes, however, will require more advanced models than those discussed herein; you can find more details in a textbook like [176].

Leverett J-*Function*

To use the relation between capillary pressure and saturation in practical modeling, it is convenient to express the capillary–saturation relationship $P_c(S_w)$ as an explicit or tabulated function. In the petroleum industry, one usually uses flooding experiments on core samples from the reservoir to develop empirical models based on observations of the relationship between average p_c and S_w values inside the core models. Each core sample will naturally generate a different capillary curve because of differences in pore-size distribution, porosity, and permeability. To normalize the measured data, it is common to use a so-called *Leverett* J-*function* [184], which takes the form

$$J(S_w) = \frac{P_c}{\sigma \cos\theta}\sqrt{\frac{K}{\phi}}. \tag{8.9}$$

Here, the surface tension σ and the contact angle θ are measured in the laboratory and are specific to a particular rock and fluid system. The scaling factor $\sqrt{K/\phi}$ is proportional to the characteristic, effective pore-throat radius. The function J can now be obtained as a (tabulated) function of S_w by fitting rescaled observed data (p_c and s_w) to a strictly monotone J-shaped function. Then, the resulting function is used to extrapolate capillary pressure data measured for a given rock to rocks that are similar, but have different permeability, porosity, and wetting properties. One cannot expect to find a J function that is generally applicable because the parameters that affect capillary pressure vary largely with rock type. Nevertheless, experience has shown that J-curves correlate well for a given rock type and in reservoir models it is therefore common to derive a J-curve for each specific rock type (facies)[1] that is represented in the underlying geological model.

To set up a multiphase flow simulation, we need the initial saturation distribution inside the reservoir. If we know the location of the OWC, the saturation higher up in the formation can be determined by combining (8.7) and (8.9)

$$S_w = J^{-1}\Big(\frac{\Delta\rho g h}{\sigma\cos\theta}\sqrt{\frac{K}{\phi}}\Big).$$

Other Relationships

In other application areas than petroleum recovery, it is common to use models that express the capillary pressure directly as an explicit function of the normalized (or effective) water saturation,

[1] By (litho)facies, we mean a part of the rock that is distinguishable by its texture, mineralogy, grain size, and the depositional environment that produced it.

https://doi.org/10.1017/9781108591416.012 Published online by Cambridge University Press

$$\hat{S}_w = \frac{S_w - S_w^{\min}}{S_w^{\max} - S_w^{\min}}. \tag{8.10}$$

Here, $S_w^{\max}$ and $S_w^{\min}$ are the maximum and minimum values the saturation can attain during the displacement. For the primary drainage shown to the left in Figure 8.4, it is natural to set $S_w^{\max} = 1$ and $S_w^{\min} = S_{wr}$, whereas $S_w^{\max} = 1 - S_{or}$ and $S_w^{\min} = S_{wr}$ for all subsequent displacements. The following model was proposed by Brooks and Corey [54] to model the relationship between capillary pressure and water saturation in partially saturated media (i.e., in the vadoze zone where the two-phase flow consists of water and air; see Section 8.3.5):

$$\hat{S}_w = \begin{cases} (p_c/p_e)^{-n_b}, & \text{if } p_c > p_e, \\ 1, & p_c \leq p_e. \end{cases} \tag{8.11}$$

Here, p_e is the entry pressure of air and $n_b \in [0.2, 5]$ is a parameter related to the pore-size distribution. Another classical model is the one proposed by van Genuchten [298]:

$$\hat{S}_w = \left(1 + \left(\beta_g p_c\right)^{n_g}\right)^{-m_g}, \tag{8.12}$$

where β_g is a scaling parameter related to the average size of pores and the exponents n_g and m_g are related to the pore-size distribution.

8.1.4 Relative Permeability

When discussing incompressible, single-phase flow, we saw that the only petrophysical parameter affecting how fast a fluid flows through a porous medium is the absolution permeability $\mathbf{K}$ that measures the capacity of the rock to transmit fluids, or alternatively the resistance the rock offers to flow. As described in Chapters 2 and 4, absolute permeability is an intrinsic property of the rock and does not depend on the type of fluid that flows through the rock. In reality, this is not true, mainly because of microscale interactions between rock and fluid may cause particles to move, pore spaces to be plugged, clays to swell when brought in contact with water, etc. Likewise, liquids and gases may not necessarily experience the same permeability, because gas does not adhere to the mineral surfaces in the same way as liquids do. This means that whereas the flow of liquids is subject to no-slip boundary conditions, gases may experience slippage that gives a pressure-dependent apparent permeability, which at low flow rates is higher than the permeability experienced by liquids. This is called the *Klinkenberg effect* and plays a substantial role for gas flows in low-permeable, unconventional reservoirs such as coal seams, tight sands, and shale formations. Herein, we will not consider reservoirs where these effects are pronounced and henceforth, we assume – as for the incompressible, single-phase flow models in Chapter 4 – that the absolute permeability $\mathbf{K}$ is an intrinsic quantity.

When more than one phase is present in the pore space, each phase α will experience an effective permeability $\mathbf{K}_\alpha^e$ that is less than the absolute permeability $\mathbf{K}$. Looking at the

https://doi.org/10.1017/9781108591416.012 Published online by Cambridge University Press

conceptual drawing in Figure 8.1, it is easy to see why this is so. The presence of another phase will effectively present additional "obstacles," whose interfacial tension offers resistance to flow. Because interfacial tension exists between all immiscible phases, the sum of all the effective phase permeabilities will generally be less than one, i.e.,

$$\sum_{\alpha} \mathbf{K}_{\alpha}^{e} < \mathbf{K}.$$

To model this reduced permeability, we introduce a property called *relative permeability* [219], which for an isotropic medium is defined as

$$k_{r\alpha} = K_{\alpha}^{e}/K. \tag{8.13}$$

Because the effective permeability is always less than or equal to the absolute permeability, $k_{r\alpha}$ will take values in the interval between 0 and 1. For anisotropic media, the relationship between the effective and absolution permeability may in principle be different for each component of the tensors. However, it is still common to define the relative permeability as a scalar quantity postulated to be in the form

$$\mathbf{K}_{\alpha}^{e} = k_{r\alpha}\mathbf{K}. \tag{8.14}$$

Relative permeabilities will generally be functions of saturation, which means that for a two-phase system we can write

$$k_{rn} = k_{rn}(S_n) \quad \text{and} \quad k_{rw} = k_{rw}(S_w).$$

It is important to note that the relative permeabilities generally are nonlinear functions of the saturations, so that the sum of these functions at a specific location (with a specific composition) is not necessarily equal to one. As for the relationship between saturation and capillary pressure, the relative permeabilities are strongly dependent on the lithofacies. It is therefore common practice to associate a unique pair of curves with each rock type represented in the geological model. Relative permeabilities may also depend on pore-size distribution, fluid viscosity, and temperature, but these factors are usually ignored in models of conventional reservoirs.

In simplified models, it is common to assume that $k_{r\alpha}$ are monotone functions that assume unique values in $[0, 1]$ for all values $S_\alpha \in [0, 1]$, so that $k_{r\alpha} = 1$ corresponds to the case with fluid α occupying the entire pore space, and $k_{r\alpha} = 0$ when $S_\alpha = 0$; see the left plot in Figure 8.5. In practice, $k_{r\alpha} = 0$ occurs when the fluid phase becomes immobilized for $S_\alpha \leq S_{\alpha r}$, giving relative permeability curves as shown in the right plot in Figure 8.5. The preferential wettability can be deducted from the point where two curves cross. Here, the curves cross for $S_w > 0$, which indicates that the system is water-wet.

Going back to our previous discussion of hysteresis, we generally expect relative permeability to be different during drainage and imbibition. The drainage curve in Figure 8.6 corresponds to the primary drainage process discussed in connection with Figure 8.4, in which a non-wetting hydrocarbon phase migrates into a water-wetting porous medium completely saturated by water. After water has been drained to its irreducible saturation,

https://doi.org/10.1017/9781108591416.012 Published online by Cambridge University Press

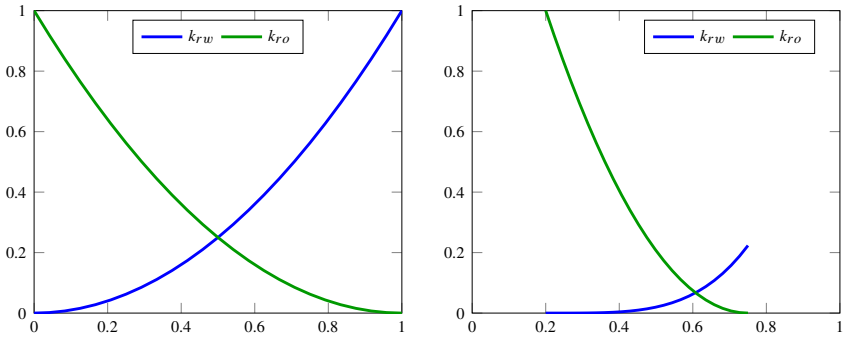

Figure 8.5 Illustration of relative permeabilities for a two-phase system. The left plot shows an idealized system with no residual saturations, while the right plot shows more realistic curves from a water-wet system.

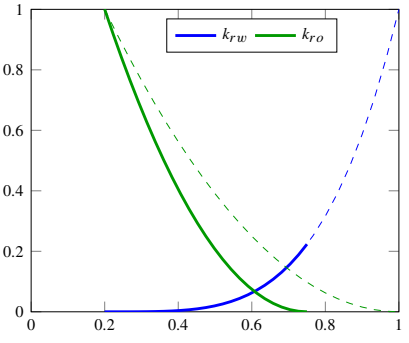

Figure 8.6 Illustration of relative permeability hysteresis, with drainage curves shown as thin, dashed lines and imbibition curves shown as thick lines.

water is reinjected to flush out the oil. In this particular illustration, the relative permeability of water k_{rw} exhibits no hysteretic behavior, whereas the imbibition and drainage curves deviate significantly for k_{ro}.

Two-Phase Relative Permeability

It is quite common to use simple analytic relationships to represent relative permeabilities. These are usually stated using the normalized or effective saturation $\hat{S}_w$ from (8.10). The simplest model possible is a pure power-law relationship, which is sometimes called a Corey model,

$$k_{rw} = \left(\hat{S}_w\right)^{n_w} k_w^0, \qquad k_{ro} = \left(1 - \hat{S}_w\right)^{n_o} k_o^0, \tag{8.15}$$

where the exponents $n_w, n_o \geq 1$ and the constants k_α^0 used for end-point scaling, should be fit to measured data. Another popular choice is the use of the Brooks–Corey functions

https://doi.org/10.1017/9781108591416.012 Published online by Cambridge University Press

$$k_{rw} = \left(\hat{S}_w\right)^{n_1+n_2n_3}, \qquad k_{ro} = \left(1-\hat{S}_w\right)^{n_1}\left[1-\left(\hat{S}_w\right)^{n_2}\right]^{n_3}, \tag{8.16}$$

where $n_1 = 2$, $n_2 = 1 + 2/n_b$, and $n_4 = 1$ gives the Brooks–Corey–Burdine model and $n_1 = \eta$, $n_2 = 1 + 1/n_b$, and $n_3 = 2$ gives the Brooks–Corey–Mualem model. It is also possible to derive models that correspond with the van Genuchten capillary functions in (8.12). In the case that $m_g = 1 - 1/n_g$, this reads

$$\begin{aligned} k_{rw} &= \hat{S}_w^{\kappa}\left[1-(1-\hat{S}_w^{1/m_g})^{m_g}\right]^2, \\ k_{ro} &= (1-\hat{S}_w)^{\kappa}\left[1-\hat{S}_w^{1/m_g}\right]^{2m_g}, \end{aligned} \tag{8.17}$$

where the connectivity factor κ is a fitting parameter. This is called the van Genuchten–Mualem model, whereas the closed-form expressions obtained for $m_g = 1 - 2/n_g$,

$$\begin{aligned} k_{rw} &= \hat{S}_w^{2}\left[1-(1-\hat{S}_w^{1/m_g})^{m_g}\right], \\ k_{ro} &= (1-\hat{S}_w)^{2}\left[1-\hat{S}_w^{1/m_g}\right]^{m_g}, \end{aligned} \tag{8.18}$$

is called the van Genuchten–Burdine model.

Three-Phase Relative Permeability

Measuring relative permeability has traditionally been costly and complex. Recently, laboratory techniques have made great progress by using computer tomography and nuclear magnetic resonance (NMR) to scan the test cores where the actual phases are being displaced. Although standard experimental procedures exist for measuring relative permeabilities in two-phase systems, there is nevertheless still significant uncertainty concerning the relevance of the experimental values found, and it is difficult to come up with reliable data to be used in a simulator. This is mainly due to boundary effects. Particularly for three-phase systems, there is a lot of uncertainty in reported data (see the review by [29]) and it is not unfair to say that no reliable experimental technique exists. Thus, three-phase relative permeabilities are usually modeled using two-phase measurements, for which several theoretical models have been proposed. Most of them are based on an idea first proposed by Stone [282], and seek to combine sets of two-phase relative permeabilities to give three-phase relationships.

In Stone's original model, which was developed for water-wet porous media and is commonly referred to as the Stone I model, the idea was that the relative permeability of water and gas would be identical to the models measured in water/oil displacements and oil/gas displacements, respectively. In the following, I use the convention that k^{wo} denotes a relationship derived from water/oil displacements and k^{og} are relationships derived from oil/gas displacements. Hence, we have that

$$k_{rw}(S_w) = k_{rw}^{wo}(S_w) \qquad k_{rg}(S_g) = k_{rg}^{go}(S_g). \tag{8.19}$$

https://doi.org/10.1017/9781108591416.012 Published online by Cambridge University Press

The three-phase relative permeability of oil, on the other hand, depends nonlinearly on both water and gas saturations,

$$k_{ro}(S_w, S_g) = \frac{\hat{S}_o}{k_{ro}^{wo}(S_{wc})} \frac{k_{ro}^{wo}(S_w)}{1 - \hat{S}_w} \frac{k_{ro}^{og}(S_g)}{1 - \hat{S}_g}. \tag{8.20}$$

Here, we have introduced the following scaled quantities

$$\begin{aligned} \hat{S}_o &= \frac{S_o - S_{om}}{1 - S_{wc} - S_{om}}, && \text{for } S_o \geq S_{om} \\ \hat{S}_w &= \frac{S_w - S_{wc}}{1 - S_{wc} - S_{om}}, && \text{for } S_w \geq S_{wc} \\ \hat{S}_g &= \frac{S_g}{1 - S_{wc} - S_{om}}. \end{aligned}$$

Here, S_{wc} is the connate water saturation and S_{om} is the minimum oil saturation. To close the model, we can for instance use the expression for S_{om} given by Fayers and Matthews [109]

$$S_{om} = \alpha S_{orw} + (1 - \alpha) S_{org}, \qquad \alpha = 1 - S_g/(1 - S_{wc} - S_{org}), \tag{8.21}$$

where S_{orw} and S_{org} denote the residual oil saturations for waterflooding and gasflooding, respectively.

Stone later proposed an alternative expression for the relative permeability of oil called the Stone II model [283]. A number of modifications and alternative formulations have been developed over the years; see, e.g., [29] for a review. MRST implements a different model that uses a linear relationship to interpolate the two-phase curves. This is the same model as the default choice in the commercial ECLIPSE simulator [271], and will be discussed in more detail in Section 11.3.

8.2 Flow Equations for Multiphase Flow

Having introduced the new physical parameters and key phenomena that characterize multiphase flow of immiscible fluids, we are in a position to develop mathematical models describing multiphase flow. To this end, we follow more or less the same steps as we did for single-phase flow in Section 4.2. Stating the generic equations describing multiphase flow is straightforward and will result in a system of partial differential equations that contains more unknowns than equations. The system must hence be extended with constitutive equations to relate the various physical quantities, as well as boundary conditions and source terms (see Sections 4.3.1 and 4.3.2) that describe external forces driving the flow. However, as indicated in the introduction of the chapter, the generic flow model has a complex mathematical character and contains delicate balances of various physical forces, whose characteristics and individual strengths vary a lot across different flow regimes. To reveal the mathematical character, but also to make models that are more computationally

https://doi.org/10.1017/9781108591416.012 Published online by Cambridge University Press

tractable in practical simulations, you need to develop more specific models that apply under certain assumptions on the flow regimes.

8.2.1 Single-Component Phases

To develop a generic system of flow equations for multiphase flow, we use the fundamental principle of mass conservation. For N immiscible fluid phases that each consists of a single component, we write one conservation equation per phase,

$$\frac{\partial}{\partial t}\left(\phi\rho_\alpha S_\alpha\right) + \nabla\cdot\left(\rho_\alpha\vec{v}_\alpha\right) = \rho_\alpha q_\alpha. \tag{8.22}$$

Here, each phase can contain multiple chemical species, but these can be considered as a single component since there is no transfer between the phases so that their composition remains constant in time.

As for the flow of a single fluid, the primary constitutive relationship used to form a closed model is Darcy's law (4.2), which can be extended to multiphase flow by using the concept of relative permeabilities discussed above

$$\vec{v}_\alpha = -\frac{\mathbf{K}k_{r\alpha}}{\mu_\alpha}(\nabla p_\alpha - g\rho_\alpha\nabla z). \tag{8.23}$$

This extension of Darcy's law to multiphase flow is often attributed to Muskat and Wyckoff [219] and has only been rigorously derived from first principles in the case of two fluid phases. Equation (8.23) must therefore generally be considered as being phenomenological. Darcy's law is sometimes stated with the opposite sign for the gravity term, but herein we use the convention that g is a positive constant. Likewise, it is common to introduce phase mobilities $\boldsymbol{\lambda}_\alpha = \mathbf{K}k_{r\alpha}/\mu_\alpha$ or relative phase mobilities $\boldsymbol{\lambda}_\alpha = \lambda_\alpha\mathbf{K}$ to simplify the notation slightly. From the discussion in the previous section, we also have an additional closure relationship stating that the saturations sum to zero (8.1), as well as relations of the form (8.8) that relate the pressures of the different phases by specifying the capillary pressures as functions of the fluid saturations.

Most commercial reservoir simulators compute approximate solutions by inserting the multiphase Darcy equations (8.23) into (8.22), introducing functional relationships for capillary pressure and how ρ_α and ϕ depend on phase pressure, and then discretizing the resulting conservation equations more or less directly. If we use the discrete derivative operators from Section 4.4.2, combined with a backward discretization of the temporal derivatives, the resulting system of fully implicit, discrete equations for phase α reads

$$\frac{(\boldsymbol{\phi}\boldsymbol{S}_\alpha\boldsymbol{\rho}_\alpha)^{n+1} - (\boldsymbol{\phi}\boldsymbol{S}_\alpha\boldsymbol{\rho}_\alpha)^n}{\Delta t^n} + \mathtt{div}(\boldsymbol{\rho}\boldsymbol{v})_\alpha^{n+1} = (\boldsymbol{\rho}\boldsymbol{q})_\alpha^{n+1}, \tag{8.24a}$$

$$\boldsymbol{v}_\alpha^{n+1} = -\frac{\boldsymbol{K}\boldsymbol{k}_{r\alpha}}{\boldsymbol{\mu}_\alpha^{n+1}}\left[\mathtt{grad}(\boldsymbol{p}_\alpha^{n+1}) - g\boldsymbol{\rho}_\alpha^{n+1}\mathtt{grad}(\boldsymbol{z})\right], \tag{8.24b}$$

Here, $\boldsymbol{\phi}, \boldsymbol{S}_\alpha, \boldsymbol{p}_\alpha \in \mathbb{R}^{n_c}$ denote vectors with one porosity value, one saturation, and one pressure value per cell, respectively, whereas $\boldsymbol{v}_\alpha$ is the vector of fluxes for phase α per

https://doi.org/10.1017/9781108591416.012 Published online by Cambridge University Press

face, and so on. For properties depending on pressure and saturation, we have for simplicity not introduced any notation to distinguish whether these are evaluated in cells or at cell interfaces. The superscript refers to discrete times and Δt denotes the associated time step.

The main advantage of using this direct discretization is that it will generally give a reasonable approximation to the true solution as long as we are able to solve the resulting nonlinear system at each time step. To do this, we must pick as many unknowns as we have phases and perform some kind of linearization; we will come back in more detail later in the book, and discuss implementation of (8.24) in Chapter 11. Here, we simply observe that there are many ways to perform the linearization: we can choose the phase saturations as primary unknowns, the phase pressures, the capillary pressures, or some combinations thereof. How difficult it will be to solve for these unknowns will obviously depend on the coupling between the two equations and nonlinearity within each equation. The main disadvantages of discretizing (8.22) directly are that the general system conceals its mathematical nature and that the resulting equations are not well-posed in the case of an incompressible system. In Section 8.3, we will therefore go back to the continuous equations and analyze the mathematical nature of the resulting system for various choices of primary variables and simplifying assumptions.

8.2.2 Multicomponent Phases

In many cases, each phase may consist of more than one chemical species that are mixed at the molecular level and generally share the same velocity (and temperature). This type of flow differs from the immiscible case, since dispersion and Brownian motion will cause the components to redistribute if there are macroscale gradients in the mass fractions. The simplest way to model this is through a linear Fickian diffusion,

$$\vec{J}_\alpha^\ell = -\rho_\alpha S_\alpha \mathbf{D}_\alpha^\ell \nabla c_\alpha^\ell, \tag{8.25}$$

where c_α^ℓ is the mass fraction of component ℓ in phase α, ρ_α is the density of phase α, S_α is the saturation of phase α, and $\mathbf{D}_\alpha^\ell$ is the diffusion tensor for component ℓ in phase α. Likewise, the chemical species may interact and undergo chemical reactions, but a description of this is beyond the scope of this book.

For multicomponent, multiphase flow, we are, in principle, free to choose whether we state the conservation of mass for components or for fluid phases. However, if we choose the latter, we will have to include source terms in our balance equations that account for the transfer of components between the phases. This can be a complex undertaking and the standard approach is therefore to develop balance equations for each component. For a system of N fluid phases and M chemical species, the mass conservation for component $\ell = 1, \ldots, M$ reads

https://doi.org/10.1017/9781108591416.012 Published online by Cambridge University Press

$$\frac{\partial}{\partial t}\Big(\phi \sum_{\alpha} c_{\alpha}^{\ell}\rho_{\alpha}S_{\alpha}\Big) + \nabla\cdot\Big(\sum_{\alpha} c_{\alpha}^{\ell}\rho_{\alpha}\vec{v}_{\alpha} + \vec{J}_{\alpha}^{\ell}\Big) = \sum_{\alpha} c_{\alpha}^{\ell}\rho_{\alpha}q_{\alpha}, \tag{8.26}$$

where $\vec{v}_\alpha$ is the superficial phase velocity and q_α is the source term. The system is closed in the same way as for single-component phases, except that we now also have to use that the mass fractions sum to zero, (8.3).

The generic system (8.23)–(8.26) can also describe miscible displacements in which the composition of the fluid phases changes when the porous medium undergoes pressure and saturation changes and one has to account for all, or a large majority, of the chemical species that are present in the flow system. For immiscible or partially miscible systems, it is common to introduce simplifications by lumping multiple species into pseudo-components, or even disregard that a fluid phase may be composed of different chemical species, as we will see next.

8.2.3 Black-Oil Models

The most common approach to simulate oil and gas recovery is to use the so-called black-oil equations, which essentially constitute a special multicomponent model with no diffusion among the components. The name refers to the assumption that the chemical species can be lumped together to form two *pseudo-components* at surface conditions, a heavy hydrocarbon component called "oil" and a light hydrocarbon component called "gas." At reservoir conditions, the two components can be partially or completely dissolved in each other depending on pressure and temperature, forming either one or two phases: a liquid oleic phase and a gaseous phase. In addition to the two hydrocarbon phases, the framework includes an aqueous phase that in the simplest models of this class is assumed to consist of only water. In more comprehensive models, the hydrocarbon components are also allowed to dissolve in the aqueous phase and the water component may be dissolved or vaporized in the two hydrocarbon phases. The composition of each hydrocarbon component, however, remains constant for all times.

We henceforth assume three phases (oleic, gaseous, and aqueous) and three components (oil, gas, and water). By looking at our model (8.23)–(8.26), we see that we so far have introduced 27 unknown physical quantities: 9 mass fractions c_α^ℓ and 3 of each of the following six quantities: ρ_α, S_α, $\vec{v}_\alpha$, p_α, μ_α, and $k_{r\alpha}$. In addition, the porosity will typically depend on pressure as discussed in Section 2.4.1. To determine these 27 unknowns, we have 3 continuity equations (8.26), an algebraic relation for the saturations (8.1), 3 algebraic relations for the mass fractions (8.3), and Darcy's law (8.23) for each of the 3 phases. Altogether, this constitutes only 10 equations. Thus, we need to add 17 extra closure relations to make a complete model.

The first five of these can be obtained immediately from our discussion in Sections 8.1.3 and 8.1.4, where we saw that the relative permeabilities $k_{r\alpha}$ are functions of the phase saturations. Likewise, capillary pressures are functions of saturation and can be used to relate phase pressures as follows:

https://doi.org/10.1017/9781108591416.012 Published online by Cambridge University Press

$$p_o - p_w = P_{cow}(S_w, S_o), \qquad p_g - p_o = P_{cgo}(S_o, S_g).$$

The required functional forms are normally obtained from a combination of physical experiments, small-scale numerical simulations, and analytical modeling based on bundle-of-tubes arguments, etc. Viscosities are either assumed to be constant or can be established as pressure-dependent functions through laboratory experiments, which gives us another three equations. The remaining nine closure relations are obtained from mixture rules and PVT models that are generalizations of the equations of state discussed in Section 4.2.

By convention, the black-oil equations are formulated as conservation for the oil, water, and gas components. To this end, we employ a simple PVT model that uses pressure-dependent functions to relate fluid volumes at reservoir and surface conditions. Specifically, we use the *formation-volume factors* $B_\ell = V_\ell / V_{\ell s}$ that relate the volumes V_ℓ and $V_{\ell s}$ occupied by a bulk of component ℓ at reservoir and surface conditions, respectively. The formation-volume factors, and their reciprocal *shrinkage factors* $b_\ell = V_{\ell s}/V_\ell$, which I personally prefer to use for notational convenience, are assumed to depend on phase pressure. In dead-oil systems, the oil is at such a low pressure that it does not contain any gas or has lost its volatile components (which presumably have escaped from the reservoir). Neither of the components are therefore dissolved in the other phases at reservoir conditions. In live-oil systems, gas is dissolved in the oleic phase. When underground, hydrocarbon molecules are mostly in liquid phase, but gaseous components are liberated when the oil is pumped to the surface. The solubility of gas in oil is usually modeled through the pressure-dependent solution gas–oil ratio, $R_s = V_{gs}/V_{os}$, defined as the volume of gas, measured at standard conditions, that at reservoir conditions is dissolved in a unit of stock-tank oil. In condensate reservoirs, oil is vaporized in the gaseous phase, so that when underground, condensate oil is mostly a gas, but condenses into a liquid when pumped to the surface. The solubility of oil in gas is modeled as the pressure-dependent vaporized oil–gas ratio R_v, defined as the amount of surface condensate that can be vaporized in a surface gas at reservoir conditions. Using this notation,[2] the black-oil equations for a live-oil system reads,

$$\begin{aligned}
\partial_t\big[\phi\big(b_o S_o + b_g R_v S_g\big)\big] + \nabla\cdot\big(b_o\vec{v}_o + b_g R_v \vec{v}_g\big) - \big(b_o q_o + b_g R_v q_g\big) &= 0,\\
\partial_t\big(\phi b_w S_w\big) + \nabla\cdot\big(b_w\vec{v}_w\big) - b_w q_w &= 0,\\
\partial_t\big[\phi\big(b_g S_g + b_o R_s S_o\big)\big] + \nabla\cdot\big(b_g\vec{v}_g + b_o R_s \vec{v}_o\big) - \big(b_g q_g + b_o R_s q_o\big) &= 0.
\end{aligned}$$

To model enhanced oil recovery, we must extend the system with additional components representing chemical or microbial species that are added to the injected fluids to mobilize immobile oil by altering wettability and/or to improve sweep efficiency and hence the overall displacement of mobile oil. One may also model species dissolved in the resident fluids. Likewise, the black-oil equations may be expanded by an additional solid phase to account for salts and other minerals that precipitate during hydrocarbon recovery, and possibly also extended to include an energy equation that accounts for temperature effects.

[2] The convention in the petroleum literature is to use B_α rather than b_α.

https://doi.org/10.1017/9781108591416.012 Published online by Cambridge University Press

We will return to a more detailed discussion of the general case of three-phase flow with components that may transfer between phases later in Chapter 11. In the rest of this chapter, we continue to study the special case of two single-component fluid phases with no interphase mass transfer.

8.3 Model Reformulations for Immiscible Two-Phase Flow

For the special case of two immiscible fluids, found in a wetting w and a non-wetting n phase, the general system of flow equations (8.22) simplifies to

$$\begin{aligned} \frac{\partial}{\partial t}(\phi S_w \rho_w) + \nabla \cdot (\rho_w \vec{v}_w) &= \rho_w q_w, \\ \frac{\partial}{\partial t}(\phi S_n \rho_n) + \nabla \cdot (\rho_n \vec{v}_n) &= \rho_n q_n. \end{aligned} \tag{8.27}$$

In the following, we discuss various choices of primary variables and how these choices affect the mathematical structure of the resulting coupled system of nonlinear differential equations.

8.3.1 Pressure Formulation

If we choose the phase pressures p_n and p_w as primary unknowns, we must express the saturations S_n and S_w as functions of pressure. To this end, we assume that the capillary pressure has a unique inverse function $\hat{S}_w = P_c^{-1}(p_c)$ (see (8.8)) so that we can write

$$S_w = \hat{S}_w(p_n - p_w), \qquad S_n = 1 - \hat{S}_w(p_n - p_w). \tag{8.28}$$

Then, we can reformulate (8.27) as

$$\begin{aligned} \frac{\partial}{\partial t}(\phi \rho_w \hat{S}_w) + \nabla \cdot \Big(\frac{\rho_w \mathbf{K} k_{rw}(\hat{S}_w)}{\mu_w} \big(\nabla p_w - \rho_w g \nabla z \big) \Big) &= \rho_w q_w, \\ \frac{\partial}{\partial t}(\phi \rho_n (1 - \hat{S}_w)) + \nabla \cdot \Big(\frac{\rho_n \mathbf{K} k_{rn}(\hat{S}_w)}{\mu_n} \big(\nabla p_n - \rho_n g \nabla z \big) \Big) &= \rho_n q_n. \end{aligned} \tag{8.29}$$

This system is unfortunately highly coupled and strongly nonlinear. The strong coupling comes from the fact that the difference in the primary variables $p_n - p_w$ enters the computation of $\hat{S}_w$ in the accumulation terms and also appears in the composite functions $k_{rw}(\hat{S}_w(\cdot))$ and $k_{rn}(1 - \hat{S}_w(\cdot))$ used to evaluate the relative permeabilities. As an example of the resulting nonlinearity, we can look at the van Genuchten model for capillary and relative permeabilities, (8.12) and (8.17). Figure 8.7 shows the capillary pressure and relative permeabilities as functions of S as well as the inverse of the capillary pressure and relative permeabilities as functions of $p_n - p_w$. Whereas the accumulation function is nonlinear, this nonlinearity is further accentuated when used inside the nonlinear relative permeability functions. The pressure formulation was used in the simultaneous solution scheme originally proposed by Douglas, Peaceman, and Rachford [86] in 1959, but has

https://doi.org/10.1017/9781108591416.012 Published online by Cambridge University Press

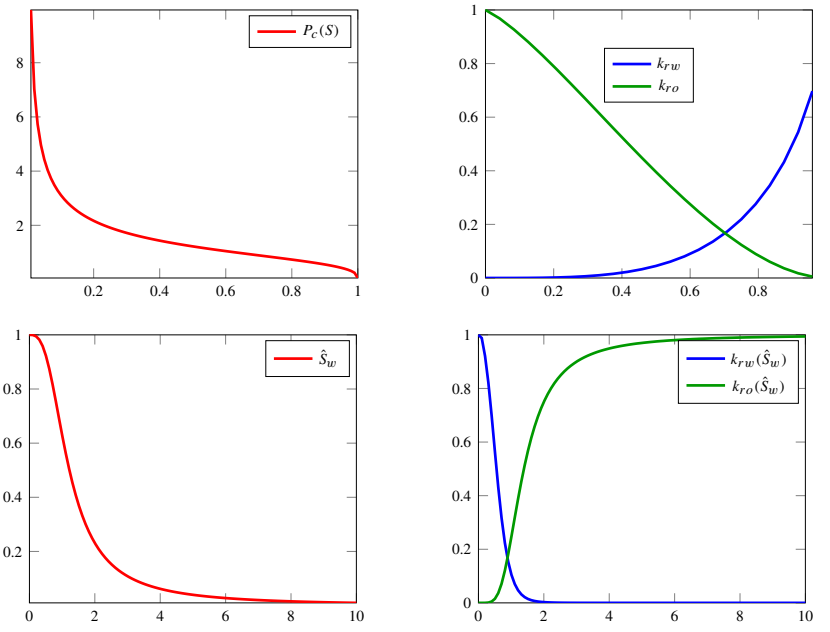

Figure 8.7 Capillary pressure and relative permeabilities as functions of S for the van Genuchten model for $\beta_g = 1$, $m_g = 2/3$, and $\kappa = 1/2$. The lower row shows saturation and relative permeabilities as function of $p_c = p_n - p_w$.

later been superseded by other formulations that reduce the degree of coupling and improve the nonlinear nature of the equation.

8.3.2 Fractional-Flow Formulation in Phase Pressure

The strong coupling and much of the nonlinearity seen in the previous formulation can be eliminated if we instead express the system in terms of one phase pressure and one phase saturation. A common choice is to use p_n and S_w, which gives the following system

$$\begin{aligned}\frac{\partial}{\partial t}(\phi S_w \rho_w) + \nabla \cdot \Big(\frac{\rho_w \mathbf{K} k_{rw}}{\mu_w} \big(\nabla p_n - \nabla P_c(S_w) - \rho_w g \nabla z \big) \Big) &= \rho_w q_w, \\ \frac{\partial}{\partial t}(\phi (1 - S_w) \rho_n) + \nabla \Big(\frac{\rho_n \mathbf{K} k_{rn}}{\mu_n} \big(\nabla p_n - \rho_n g \nabla z \big) \Big) &= \rho_n q_n. \end{aligned} \tag{8.30}$$

To further develop this system of equations, it is common to expand the derivatives to introduce rock and fluid compressibilities, as discussed for the single-phase flow equation in Section 4.2. First, however, we will look closer at the special case of incompressible flow and develop the *fractional-flow formulation*, which will enable us to further expose the mathematical structure of the system.

https://doi.org/10.1017/9781108591416.012 Published online by Cambridge University Press

Incompressible Flow

For incompressible flow, the porosity ϕ only varies in space and the fluid densities ρ_α are constant. Using these assumptions, we can simplify the mass-balance equations to be on the form

$$\phi \frac{\partial S_\alpha}{\partial t} + \nabla \cdot \vec{v}_\alpha = q_\alpha. \tag{8.31}$$

To derive the fractional-flow formulation, we start by introducing the total Darcy velocity, which we can express in terms of the pressure for the non-wetting phase,

$$\begin{aligned} \vec{v} = \vec{v}_n + \vec{v}_w &= -\boldsymbol{\lambda}_n \nabla p_n - \boldsymbol{\lambda}_w \nabla p_w + (\boldsymbol{\lambda}_n \rho_n + \boldsymbol{\lambda}_w \rho_w) g \nabla z \\ &= -(\boldsymbol{\lambda}_n + \boldsymbol{\lambda}_w) \nabla p_n + \boldsymbol{\lambda}_w \nabla p_c + (\boldsymbol{\lambda}_n \rho_n + \boldsymbol{\lambda}_w \rho_w) g \nabla z. \end{aligned} \tag{8.32}$$

We then add the two continuity equations and use the fact that $S_n + S_w = 1$ to derive a pressure equation without temporal derivatives

$$\nabla \cdot (\vec{v}_n + \vec{v}_w) = \nabla \cdot \vec{v} = q_n + q_w \tag{8.33}$$

If we now define the total mobility $\boldsymbol{\lambda} = \boldsymbol{\lambda}_n + \boldsymbol{\lambda}_w = \lambda \mathbf{K}$ and total source $q = q_n + q_w$, insert (8.32) into (8.33), and collect all terms that depend on pressure on the left-hand side and all other terms on the right-hand side, we obtain an elliptic Poisson-type equation

$$-\nabla \cdot (\lambda \mathbf{K} \nabla p_n) = q - \nabla \big[\boldsymbol{\lambda}_w \nabla p_c + (\boldsymbol{\lambda}_n \rho_n + \boldsymbol{\lambda}_w \rho_w) g \nabla z \big]. \tag{8.34}$$

This *pressure equation* (or flow equation) is essentially on the same form as the equation (4.10) governing single-phase, incompressible flow, except that both the variable coefficient and the right-hand side now depend on saturation through the relative mobility λ and the capillary pressure function $p_c = P_c$.

To derive an equation for S_w, we multiply each phase velocity by the relative mobility of the other phase, subtract the result, and use Darcy's law to obtain

$$\begin{aligned} \lambda_n \vec{v}_w - \lambda_w \vec{v}_n &= \lambda \vec{v}_w - \lambda_w \vec{v} \\ &= -\lambda_n \lambda_w \mathbf{K} (\nabla p_w - \rho_w g \nabla z) + \lambda_w \lambda_n \mathbf{K} (\nabla p_n - \rho_n g \nabla z) \\ &= \lambda_w \lambda_n \mathbf{K} \big[\nabla p_c + (\rho_w - \rho_n) g \nabla z \big]. \end{aligned}$$

If we now solve for $\vec{v}_w$ and insert into (8.31) for the wetting phase, we obtain what is commonly referred to as the *saturation equation* (or transport equation)

$$\phi \frac{\partial S_w}{\partial t} + \nabla \cdot \big[f_w \vec{v} + f_w \lambda_n \mathbf{K} \Delta \rho g \nabla z \big] = q_w - \nabla \cdot \big(f_w \lambda_n \mathbf{K} P_c' \nabla S_w \big). \tag{8.35}$$

Here, $\Delta \rho = \rho_w - \rho_n$, and we have introduced the *fractional flow function* $f_w = \lambda_w / (\lambda_n + \lambda_w)$, which measures the fraction of the total flow that consists of the wetting fluid.

Equation (8.35) is parabolic and accounts for the balance of three different forces: viscous advection $f_w \vec{v}$, gravity segregation $(f_w \lambda_n) \mathbf{K} \Delta \rho g \nabla z$, and capillary forces $f_w \lambda_n \mathbf{K} P_c' \nabla S_w$. The first two terms both involve a first-order derivative and hence have a *hyperbolic* character, whereas the capillary term contains a second-order derivative

https://doi.org/10.1017/9781108591416.012 Published online by Cambridge University Press

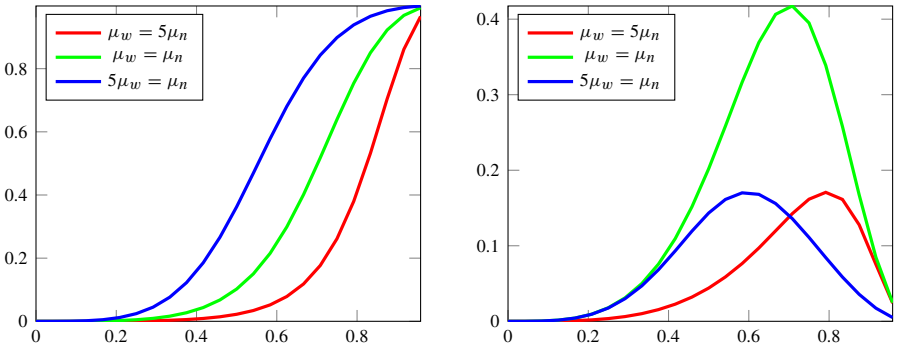

Figure 8.8 Fractional flow function f_w (left) and gravity segregation function $\lambda_n f_w$ for the van Genuchten–Mualem model (8.17) with $m_g = 2/3$, $\kappa = 1/2$, and $\Delta\rho > 0$.

and hence has a *parabolic* character. The negative sign in front of the capillary term is misleading; the overall term is positive since $P_c' < 0$ and hence gives a well-posed problem. Moreover, since λ_n is zero at the end point, the capillary term disappears at this point and the parabolic equation thus degenerates to being hyperbolic. This, in turn, implies that a propagating displacement front – in which a wetting fluid displaces a non-wetting fluid – has finite speed of propagation, and not the infinite speed of propagation that is typical for parabolic problems.

Figure 8.8 shows the functional form of the two hyperbolic terms for the van Genuchten–Mualem model (8.17). The fractional flow function f_w is monotonically increasing and has a characteristic S-shape. If the flow is dominated by viscous terms so that gravity and capillary forces are negligible, the flow will always be *cocurrent* with both phases flowing in the direction of $\vec{v}$ because the derivative of f_w is positive. The gravity segregation function, on the other hand, has a characteristic bell shape and describes the upward movement of the lighter phase and downward movement of the heavier phase. (The function is turned upside down if $\rho_w < \rho_n$.) If gravity is sufficiently strong, it may introduce *countercurrent flow*, with the fluid phases flowing in opposite directions. On a field scale, capillary forces are typically small and hence the overall transport equation will have a strong hyperbolic character. Neglecting the capillary term is generally a good approximation and gives a purely hyperbolic saturation equation. We will return to this model later and discuss a few examples in the special case of purely hyperbolic 1D flow.

The coupling between the elliptic pressure equation and the parabolic saturation equation is much weaker than the coupling between the two continuity equations in the formulation (8.29) with two pressures as primary unknowns. In the pressure equation (8.34), the coupling to saturation appears explicitly in the effective mobility, which makes up the variable coefficient in the Poisson problem, and on the right-hand side through the phase mobilities and the derivative of the capillary function. In (8.35), on the other hand, the saturation is only indirectly coupled to the pressure through the total Darcy velocity. In

https://doi.org/10.1017/9781108591416.012 Published online by Cambridge University Press

typical waterflooding scenarios, saturation variations are relatively smooth in most of the domain, except at the interface between the invading and the displaced fluids, and hence the pressure distribution is only mildly affected by the evolving fluid saturations. In fact, the pressure and transport equations are completely decoupled in the special case of linear relative permeabilities, no capillary pressure, and equal fluid densities and viscosities. These weak couplings are exploited in many efficient numerical methods, which use various forms of operator splitting to solve pressure and fluid transport in separate steps. This is also our method of choice for incompressible flow in MRST, and will be discussed in more details in Chapter 10.

The reformulation discussed above can easily be extended to N immiscible phases, and will result in one pressure equation and a (coupled) system of $N-1$ saturation equations. It is also possible to develop fractional-flow formulations for multicomponent flow without mass exchange between the phases.

Compressible Flow

To develop a fractional-flow formulation in the compressible case, we start by expanding the accumulation term in (8.22) and then use fluid compressibilities to rewrite the derivative of the phase densities

$$\begin{aligned}\frac{\partial}{\partial t}\left(\phi\rho_\alpha S_\alpha\right) &= \rho_\alpha S_\alpha\frac{\partial\phi}{\partial t} + \phi S_\alpha\frac{d\rho_\alpha}{dp_\alpha}\frac{\partial p_\alpha}{\partial t} + \phi\rho_\alpha\frac{\partial S_\alpha}{\partial t}\\ &= \rho_\alpha S_\alpha\frac{\partial\phi}{\partial t} + \phi\rho_\alpha S_\alpha c_\alpha\frac{\partial p_\alpha}{\partial t} + \phi\rho_\alpha\frac{\partial S_\alpha}{\partial t}.\end{aligned}$$

If we now insert this into (8.22), divide each equation by ρ_α, and sum the equations, we obtain

$$\frac{\partial\phi}{\partial t} + \phi c_n S_n\frac{\partial p_n}{\partial t} + \phi c_w S_w\frac{\partial p_w}{\partial t} + \frac{1}{\rho_n}\nabla\cdot\left(\rho_n\vec{v}_n\right) + \frac{1}{\rho_w}\nabla\cdot\left(\rho_w\vec{v}_w\right) = q_t, \tag{8.36}$$

where $q_t = q_n + q_w$. To explore the character of this equation, let us for the moment assume that capillary forces are negligible so that $p_n = p_w = p$ and that the spatial density variations are so small that we can set $\nabla\rho_\alpha = 0$. If we now introduce rock compressibility $c_r = d\ln(\phi)/dp$, (8.36) simplifies to

$$\phi c\frac{\partial p}{\partial t} - \nabla\cdot(\lambda\mathbf{K}\nabla p) = \hat{q}. \tag{8.37}$$

Here, we have introduced the *total compressibility* $c = (c_r + c_n S_n + c_w S_w)$ and a source function $\hat{q}$ that accounts both for volumetric sources and pressure variations with depth. Equation (8.37) is clearly parabolic, but simplifies to the elliptic Poisson equation (8.34) for incompressible flow ($c = 0$). Fluid compressibilities tend to decrease with increasing pressure, and we should therefore expect that the pressure equation has a strong elliptic character at conditions usually found in conventional reservoirs during secondary and tertiary production, in particular for weakly compressible systems. On the other hand, the pressure evolution will usually have a more pronounced parabolic character during primary

https://doi.org/10.1017/9781108591416.012 Published online by Cambridge University Press

depletion, in gas reservoirs, and in unconventional reservoirs, where $\mathbf{K}$ may be in the range of one micro Darcy or less.

These observations remain true also when capillary forces and spatial density variations are included. However, including these effects makes the mathematical structure of the equation more complicated. In particular, the pressure equation becomes a *nonlinear* parabolic equation if the spatial variations in density cannot be neglected. To see this, let us once again neglect capillary forces and consider the second-last term on the left-hand side of (8.36),

$$\begin{aligned}\frac{1}{\rho_n}\nabla\cdot(\rho_n\vec{v}) &= \nabla\cdot\vec{v}_n + \vec{v}_n\cdot\frac{1}{\rho_n}\nabla\rho_n\\ &= \nabla\cdot\vec{v}_n + \vec{v}_n\cdot\big(c_n\nabla p_n\big).\end{aligned}$$

By using Darcy's law, we can transform the inner product between the phase flux and the pressure gradient to involve a quadratic term in ∇p_n or $\vec{v}_n$,

$$\begin{aligned}\vec{v}_n\cdot\big(c_n\nabla p_n\big) &= -\boldsymbol{\lambda}_n(\nabla p_n - \rho_n g\nabla z)\cdot(c_n\nabla p_n)\\ &= c_n\vec{v}_n\cdot(-\boldsymbol{\lambda}_n^{-1}\vec{v}_n + \rho_n g\nabla z).\end{aligned}$$

The last term on the left-hand side of (8.36) has a similar form, and hence we obtain a nonlinear equation if at least one of the fluid phases has significant spatial density variations.

Going back to (8.36), we see that the equation contains both phase pressures and hence cannot be used directly alongside with a saturation equation. There are several ways to formulate a pressure equation so that it only involves a single unknown pressure. We can either pick one of the phase pressures as the primary variable, or introduce an average pressure $p_a = (p_n + p_w)/2$, as suggested in [246]. With p_n as the primary unknown, the full pressure equation reads

$$\begin{aligned}&\phi c\frac{\partial p_n}{\partial t} - \Big[\frac{1}{\rho_n}\nabla\cdot\big(\rho_n\boldsymbol{\lambda}_n\nabla p_n\big) + \frac{1}{\rho_w}\nabla\cdot\big(\rho_w\boldsymbol{\lambda}_w\nabla p_n\big)\Big]\\ &\quad= q_n + q_w - \frac{1}{\rho_w}\nabla\cdot\big(\rho_w\boldsymbol{\lambda}_w\nabla P_c\big) + c_w S_w\frac{\partial P_c}{\partial t}\\ &\qquad- \frac{1}{\rho_n}\nabla\cdot\big(\rho_n^2\boldsymbol{\lambda}_n g\nabla z\big) - \frac{1}{\rho_w}\nabla\cdot\big(\rho_w^2\boldsymbol{\lambda}_w g\nabla z\big).\end{aligned} \tag{8.38}$$

Likewise, with p_a as the primary unknown, we get

$$\begin{aligned}&\phi c\frac{\partial p_a}{\partial t} - \Big[\frac{1}{\rho_n}\nabla\cdot\big(\rho_n\boldsymbol{\lambda}_n\nabla p_a\big) + \frac{1}{\rho_w}\nabla\cdot\big(\rho_w\boldsymbol{\lambda}_w\nabla p_a\big)\Big]\\ &\quad= q_t + \frac{1}{2}\Big[\frac{1}{\rho_n}\nabla\cdot\big(\rho_n\boldsymbol{\lambda}_n\big) - \frac{1}{\rho_w}\nabla\cdot\big(\rho_w\boldsymbol{\lambda}_w\big)\Big]\nabla P_c + \tfrac{1}{2}c_w S_w\frac{\partial P_c}{\partial t}\\ &\qquad- \tfrac{1}{2}c_n S_n\frac{\partial P_c}{\partial t} - \frac{1}{\rho_n}\nabla\cdot\big(\rho_n^2\boldsymbol{\lambda}_n g\nabla z\big) - \frac{1}{\rho_w}\nabla\cdot\big(\rho_w^2\boldsymbol{\lambda}_w g\nabla z\big).\end{aligned} \tag{8.39}$$

https://doi.org/10.1017/9781108591416.012 Published online by Cambridge University Press

The same type of pressure equation can be developed for cases with more than two fluid phases. Also in this case, we can define a total velocity and use this to obtain $N-1$ transport equations in fractional-flow form.

The saturation equation for compressible flow is obtained exactly in the same way as in the incompressible case,

$$\begin{aligned}\frac{\partial}{\partial t}\big(\phi\rho_w S_w\big) + \nabla\cdot\big[\rho_w f_w\big(\vec{v} + \boldsymbol{\lambda}_n \Delta\rho g\nabla z\big)\big] \\ = \rho_w q_w - \nabla\cdot\big(\rho_w f_w \boldsymbol{\lambda}_n P_c' \nabla S_w\big).\end{aligned} \tag{8.40}$$

However, whereas total velocity was the only quantity coupling the saturation equation to the fluid pressure in the incompressible case, we now have coupling also through porosity and density, which may both depend on pressure. This generally makes the compressible case more nonlinear and challenging to solve than the incompressible case.

8.3.3 Fractional-Flow Formulation in Global Pressure

The formulation in phase pressure discussed above has a relatively strong coupling between pressure and saturation in the presence of capillary forces. The strong coupling is mainly caused by the ∇p_c term on the right-hand side of (8.34). Let us therefore go back and see if we can eliminate this term by making a different choice of primary variables. To this end, we start by looking at the definition of the total velocity, which couples the pressure to the saturation equation:

$$\begin{aligned}\vec{v} &= -\boldsymbol{\lambda}_n\nabla p_n - \boldsymbol{\lambda}_w\nabla p_w + \big(\rho_n\boldsymbol{\lambda}_n + \rho_w\boldsymbol{\lambda}_w\big)g\nabla z \\ &= -(\boldsymbol{\lambda}_n + \boldsymbol{\lambda}_w)\nabla p_n + \boldsymbol{\lambda}_w\nabla(p_n - p_w) + \big(\rho_n\boldsymbol{\lambda}_n + \rho_w\boldsymbol{\lambda}_w\big)g\nabla z \\ &= -\boldsymbol{\lambda}\big(\nabla p_n - f_w\nabla p_c\big) + \big(\rho_n\boldsymbol{\lambda}_n + \rho_w\boldsymbol{\lambda}_w\big)g\nabla z.\end{aligned}$$

If we now introduce a new pressure variable p, called the *global pressure* [62], defined so that $\nabla p = \nabla p_n - f_w\nabla p_c$, we see that the total velocity can be related to the global pressure through an equation that looks like Darcy's law

$$\vec{v} = -\boldsymbol{\lambda}\big(\nabla p - (\rho_w f_w + \rho_n f_n)g\nabla z\big). \tag{8.41}$$

By adding the continuity equations (8.31), and using (8.41), we obtain an elliptic Poisson-type equation for the global pressure

$$-\nabla\cdot\big[\lambda\mathbf{K}\big(\nabla p - (\rho_w f_w + \rho_n f_n)g\nabla z\big)\big] = q_t. \tag{8.42}$$

The advantages of this formulation is that it is very simple and highly efficient in the incompressible case, where pressure often is treated as an immaterial property and one is mostly interested in obtaining a velocity field for the saturation equation. The disadvantages are that it is not obvious how one should specify and interpret boundary conditions for the global pressure and that global-pressure values cannot be used directly in well models (of Peaceman type). The global-pressure formulation can also be extended to variable densities

https://doi.org/10.1017/9781108591416.012 Published online by Cambridge University Press

and to three-phase flow; the interested reader should consult [67, 65] and references therein. The global formulation is often used by academic researchers because of its simplicity, but is, to the best of my knowledge, hardly used for practical simulations in the industry.

8.3.4 Fractional-Flow Formulation in Phase Potential

The two fractional-flow formulations discussed above are generally well suited to study two-phase immiscible flow with small or negligible capillary forces. In such cases, flow is mainly driven through high-permeable regions, and flow paths are to a large extent determined by the permeability distribution, the shape of the relative permeability functions, and density differences (which determine the relative importance of gravity segregation). In other words, the flow is mainly governed by viscous forces and gravity segregation, which constitute the hyperbolic part of the transport equation, whereas capillary forces mostly contribute to adjust the width of the interface between the invading and displaced fluids. For highly heterogeneous media with strong contrasts in capillary functions, on the other hand, the capillary forces may have pronounced impact on flow paths by enhancing cross-flow in stratified media or reducing the efficiency of gravity drainage. Likewise, because capillary pressure is continuous across geological interfaces, differences in capillary functions between adjacent rocks of different type may introduce (strong) discontinuities in the saturation distribution.

An alternative fractional-flow formulation was proposed by Hoteit and Firoozabadi [136] to study heterogeneous media with strong contrasts in capillary functions. The formulation is similar to the ones discussed above, except that we now work with fluid potentials rather than fluid pressures. The fluid potential for phase α and the capillary potential are given by

$$\Phi_\alpha = p_\alpha - \rho_\alpha g z, \tag{8.43}$$

$$\Phi_c = \Phi_n - \Phi_w = p_c + (\rho_w - \rho_n) g z. \tag{8.44}$$

By manipulating the expression for the total velocity, we can write it as a sum of two new velocities, which each is given by the gradient of Φ_w and Φ_c, respectively:

$$\begin{aligned}
\vec{v} &= -\boldsymbol{\lambda}_n\big[\nabla p_n - \rho_n g \nabla z\big] - \boldsymbol{\lambda}_w\big[\nabla p_w - \rho_n g \nabla z\big] \\
&= -\boldsymbol{\lambda}_n\big[\nabla p_w + \nabla p_c - (\rho_n - \rho_w + \rho_w) g \nabla z\big] - \boldsymbol{\lambda}_w\big[\nabla p_w - \rho_n g \nabla z\big] \\
&= -(\boldsymbol{\lambda}_n + \boldsymbol{\lambda}_w)\big[\nabla p_w - \rho_w g \nabla z\big] - \boldsymbol{\lambda}_n\big[\nabla p_c + (\rho_w - \rho_n) g \nabla z\big] \\
&= -\boldsymbol{\lambda} \nabla \Phi_w - \boldsymbol{\lambda}_n \nabla \Phi_c = \vec{v}_a + \vec{v}_c.
\end{aligned}$$

Here, we observe that

$$\vec{v}_w = -\boldsymbol{\lambda}_w \nabla \Phi_w = -\frac{\lambda_w}{\lambda} \lambda \mathbf{K} \nabla \Phi_w, = f_w \vec{v}_a$$

so that the velocity $\vec{a}$ represents the same phase differential as the phase velocity of the wetting phase. The only exception is that in $\vec{v}_a$, the potential gradient is multiplied by the

https://doi.org/10.1017/9781108591416.012 Published online by Cambridge University Press

total mobility, which is a smoother and less varying function than the mobility λ_w of the water phase. This means that the saturation dependence of $\vec{v}_a$ is less than for the total velocity $\vec{v}$.

Proceeding analogously as above, we can derive the following coupled system for two-phase, immiscible flow:

$$-\nabla \cdot \left(\lambda \mathbf{K} \nabla \Phi_w\right) = q + \nabla \cdot \left(\lambda_n \mathbf{K} \nabla \Phi_c\right) \tag{8.45}$$

$$\phi \frac{\partial}{\partial t} + \nabla \cdot \left(f_w \vec{v}_a\right) = q_w. \tag{8.46}$$

Compared with the two other fractional-flow formulations, this system is simpler in the sense that capillary forces are only accounted for in the pressure equation. Equally important, the saturation equation is purely hyperbolic and only contains advective flow along $\vec{v}_a$. This makes the saturation much simpler to solve, since one does not have to resolve delicate balances involving nonlinear functions for gravity segregation and capillary forces. One can thus easily employ simple upwind discretizations and highly efficient solvers that have been developed for purely co-current flow, like streamline methods [79] or methods based on optimal ordering [220, 196]. On the other hand, the advective velocity $\vec{v}_a$ may vary significantly with time and hence represent a strong coupling between pressure and transport.

8.3.5 Richards' Equation

Another special case arises when modeling the vadose or unsaturated zone, which extends from the ground surface to the groundwater table, i.e., from the top of the earth to the depth at which the hydrostatic pressure of the groundwater equals one atmosphere. Soil and rock in the vadose zone will generally contain both air and water in its pores, and the vadose zone is the main factor that controls the movement of water from the ground surface to aquifers, i.e., the saturated zone beneath the water table. In the vadose zone, water is retained by a combination of adhesion and capillary forces, and in fine-grained soil one can find pores that are fully saturated by water at a pressure less than one atmosphere.

Because of the special conditions in the vadose zone, the general flow equations modeling two immiscible phases can be considerably simplified. First of all, we can expect that any pressure differences in air will be equilibrated almost instantaneously relative to water, since air typically is much less viscous than water. (At a temperature of 20 °C, the air viscosity is approximately 55 times smaller than the water viscosity.) Secondly, air will in most cases form a continuous phase so that all parts of the pore space in the vadose zone are connected to the atmosphere. If we neglect variations in the atmospheric pressure, the pore pressure of air can therefore be assumed to be constant. For simplicity, we can set the atmospheric pressure to be zero, so that $p_a = 0$ and $p_c = p_a - p_w = -p_w$. This, in turn, implies that the water saturation (and the water relative permeability) can be defined as functions of water pressure using one of the models for capillary pressure presented in Section 8.1.3. Inserting all of this into (8.27), we obtain

https://doi.org/10.1017/9781108591416.012 Published online by Cambridge University Press

$$\frac{\partial}{\partial t}\big(\phi\rho_w S_w(p_w)\big) + \nabla\cdot\big[\rho_w\lambda_{rw}(p_w)\mathbf{K}\big(\nabla p_w - \rho_w g\nabla z\big)\big] = 0.$$

If we further expand the accumulation term, neglect spatial gradients of the water density, we can divide the above equation by ρ_w to obtain the so-called *generalized Richards'* equation

$$C_{wp}(p_w)\frac{\partial p_w}{\partial t} + \nabla\cdot\big[\lambda_{rw}(p_w)\mathbf{K}\nabla(p_w - \rho g z)\big] = 0, \tag{8.47}$$

where $C_{wp} = c_w\theta_w + d(\theta_w)/dp_w$ is a storage coefficient and $\theta_w = \phi S_w$ is the water content. In hydrology, it is common to write the equation in terms of the pressure head

$$C_{wh}(h_w)\frac{\partial h_w}{\partial t} + \nabla\big[\kappa_w k_{rw}(h_w)\nabla(h_w - z)\big] = 0, \tag{8.48}$$

where $C_{wh} = \rho_w g C_{wp}$ and κ_w is the hydraulic conductivity of water (see Section 4.1 on page 113). If we further neglect water and rock compressibility, we obtain the pressure form of the classical Richards' equation [264]

$$C_{ch}(h_w)\frac{\partial h_w}{\partial t} + \nabla\big[\kappa_w k_{rw}(h_w)\nabla(h_w - z)\big] = 0, \qquad C_{ch} = \frac{d\theta_w}{dh_w}. \tag{8.49}$$

The corresponding equation for the water flux

$$\vec{v}_w = -\kappa_s k_{rw}(h_w)\nabla(h_w - z) \tag{8.50}$$

was suggested earlier by Buckingham [55] and is often called the Darcy–Buckingham equation. Richards' equation can also be expressed in two alternative forms,

$$\frac{\partial\theta_w}{\partial t} + \nabla\cdot\big[\kappa_w k_{rw}(h_w)\nabla(h_w - z)\big] = 0,$$

$$\frac{\partial\theta_w}{\partial t} + \nabla\big[\mathbf{D}(\theta_w)\nabla\theta_w\big] = \kappa_w k_{rw}(\theta_w)\nabla z,$$

where $\mathbf{D}(\theta_w) = \frac{dh_w}{d\theta_w}\kappa_w k_{rw}(\theta_w)$ is the hydraulic diffusivity tensor. The latter, called the water-content form, is generally easier to solve numerically than the other forms, but becomes infinite for fully saturated conditions.

Various forms of Richards' equation are widely used to simulate water flow in the vadose zone. However, one should be aware that this class of models has important limitations. First of all, because air pressure is assumed to be constant, these models cannot describe air flow, and also assume that the air phase in the whole pore space is fully connected to the atmosphere. This may not be the case if the porous medium contains heterogeneities blocking the air flow, e.g., in the form of layers that are almost impermeable to air. Likewise, the derivation of the equations assumed that the mobility of air is infinite compared with water, which may not be the case if the relative permeability of air is much smaller than that of water. If this is not the case, one should expect significant discrepancies in simulation results obtained from Richards' equations and the general two-phase flow equations.

The official release of MRST does not yet have any implementation of Richards' equations, but work is underway to develop a new module [299].

https://doi.org/10.1017/9781108591416.012 Published online by Cambridge University Press

8.4 The Buckley–Leverett Theory of 1D Displacements

To shed more light into the physical behavior of two-phase immiscible flow systems, we derive analytical solutions in a few simple cases. As part of this, you will also get a glimpse of the (wave) theory of hyperbolic conservation laws. This theory plays a very important role in the mathematical and numerical analysis of multiphase flow models, but is not described in great detail herein for brevity. If you want to learn more of this interesting topic, there are many good mathematical textbooks you can consult, e.g., [76, 134, 183, 293, 294]. Chapter 9 also introduces a few central concepts and briefly discusses development of specialized numerical methods.

8.4.1 Horizontal Displacement

As a first example, we consider incompressible displacement in a 1D homogeneous and horizontal medium, $x \in [0, \infty)$, with inflow at $x = 0$. In the absence of capillary forces, the two phase pressures are equal and coincide with the global pressure p. The pressure equation simplifies to

$$v'(x) = q, \qquad v(x) = -\lambda(x)p'(x).$$

If we assume that there are no volumetric source terms, but a constant inflow rate at $x = 0$, it follows by integration that $v(x)$ is constant in the domain $[0, \infty)$. Under these assumptions, the saturation equation (8.35) simplifies to,

$$\frac{\partial S}{\partial t} + \frac{v}{\phi}\frac{\partial f(S)}{\partial x} = 0. \tag{8.51}$$

Let us use this equation to study the propagation of a constant saturation value. To this end, we consider the total differential of $S(x,t)$,

$$0 = dS = \frac{\partial S}{\partial t}dt + \frac{\partial S}{\partial x}dx,$$

which we can use to eliminate $\partial S/\partial t$ from (8.51),

$$-\frac{\partial S}{\partial x}\Big(\frac{dx}{dt}\Big)\Big|_{dS=0} + \frac{v}{\phi}\frac{df}{dS}\frac{\partial S}{\partial x} = 0.$$

This gives us the following equation for the path of a value of constant saturation

$$\Big(\frac{dx}{dt}\Big)\Big|_{dS=0} = \frac{v}{\phi}\frac{df(S)}{dS}. \tag{8.52}$$

If we assume that f is a function of S only, it follows that states of constant saturation will propagate along straight lines, i.e., along paths given by

$$x(t) = x_0(t_0) + \frac{v}{\phi}\frac{df(S)}{dS}\big(t - t_0\big).$$

To make a well-posed problem, we must pose initial and boundary conditions for the saturation equation (8.51) in the form $S(x,0) = S_{0,x}(x)$ and $S(0,t) = S_{0,t}(t)$. For the special

https://doi.org/10.1017/9781108591416.012 Published online by Cambridge University Press

case of a linear fractional flow function $f(S) = S$, which corresponds to a displacement with linear relative permeabilities and equal viscotities, the analytical solution is given on closed form

$$S(x,t) = \begin{cases} S_{0,x}(x - at), & x \geq at, \\ S_{0,t}(at - x), & x < at, \end{cases}$$

where $a = v/\phi$. Loosely speaking, the interpretation of this solution is that the saturation equation takes the initial and boundary data and transports them unchanged along the x-axis with a speed a or a speed equal $f'(S)v/\phi$ in the general case. Notice that to get a classical solution, the initial and boundary data must be continuous and matching so that $S_{0,x}(0) = S_{0,t}(0)$. This way of constructing a solution is called the *method of characteristics* and has been used a lot throughout the literature of porous media to study various kinds of displacement scenarios.

Next, let us consider the case of one immiscible fluid displacing another, assuming constant initial saturation S_0 and a constant injected saturation S_i, where S_i generally is different from S_0. Without lack of generality, we set $v = \phi = 1$ or alternatively introduce new time $t^* = t\, v/\phi$ to rescale the saturation equation so that v and ϕ disappear. This gives the classical *Buckley–Leverett problem*

$$\frac{\partial S}{\partial t} + \frac{\partial f(S)}{\partial S} = 0, \qquad S(x,0) = S_0, \quad S(0,t) = S_i, \tag{8.53}$$

named after the authors [56] who first developed this type of analysis. Here, we see that all changes in saturation must originate from the jump in values from S_0 to S_i at the point $(x,t) = (0,0)$ and that these changes, which we henceforth refer to as waves, will propagate along straight lines. In (8.52), we saw that a wave corresponding to a constant S-value will propagate with a speed proportional to the derivative of the fractional flow function f. In most cases, $f(S)$ has a characteristic S-shape with one inflection point, i.e., a point at which $f'(S)$ has an isolated extremum. In essence, this means that saturation values near the extremum should travel faster than saturation values on both sides of the extremum. Thus, if we apply the characteristic equation (8.52) naively, we end up with a multivalued solution as illustrated in Figure 8.9, which is clearly not physical. Indeed, if several waves emanate from the same location in space and time, the speeds of these waves have to be non-decreasing in the direction of flow so that the faster waves move ahead of the slower waves.

We can avoid the unphysical behavior if we simply replace the multivalued solution by a discontinuity, as shown in Figure 8.9. To ensure that mass is conserved, the discontinuity can be constructed graphically so that the two shaded areas are of equal size. This, however, means that the solution cannot be interpreted in the classical sense, since derivatives are not guaranteed to exist pointwise. Instead, the solution must be defined by multiplying the saturation equation by a smooth function φ of compact support and integrating the result over time and space

$$\iint \Big[\frac{\partial S}{\partial t} + \frac{\partial f(S)}{\partial x}\Big]\varphi(x,t)\, dxdt = 0.$$

https://doi.org/10.1017/9781108591416.012 Published online by Cambridge University Press

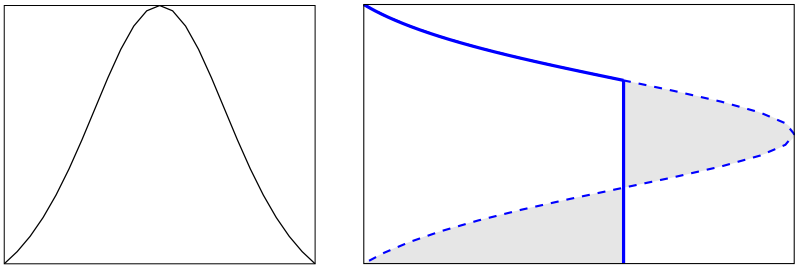

Figure 8.9 Construction of the self-similar Buckley–Leverett solution $S(x/t)$. The left plot shows $f'(S)$, whereas the right plot shows how the multivalued function given by a naive application of the characteristic equation (8.52) plotted as a dashed line is turned into a discontinuous solution plotted as a solid line by requiring that the shaded areas are of equal size.

We now integrate by parts and change the order of integration to transfer the derivatives to the smooth function φ,

$$\iint \left[S\frac{\partial \varphi}{\partial t} + f(S)\frac{\partial \varphi}{\partial x} \right] dx dt = 0. \tag{8.54}$$

A weak solution is then defined as any solution satisfying (8.54) for all smooth and compactly supported test functions φ.

In general, propagating discontinuities like the one in Figure 8.9 must satisfy certain conditions. To see this, let $x_d(t)$ denote the path of a propagating discontinuity, and pick two points x_1 and x_2 such that $x_1 < x_d(t) < x_2$. We first use the integral form of the saturation equation to write

$$f(S_1) - f(S_2) = -\int_{x_1}^{x_2} \frac{\partial f(S)}{\partial x}\, dx = \frac{d}{dt}\int_{x_1}^{x_2} S(x,t)\, dx, \tag{8.55}$$

and then decompose the last integral as follows:

$$\int_{x_1}^{x_2} S(x,t)\, dx = \lim_{\epsilon \to 0^+} \int_{x_1}^{x_d(t)-\epsilon} S(x,t)\, dx + \lim_{\epsilon \to 0^+} \int_{x_d(t)+\epsilon}^{x_2} S(x,t)\, dx.$$

Since the integrand is continuous in each of the integrals on the right-hand side of the equation, we can use the Leibniz rule to write

$$\frac{d}{dt}\int_{x_1}^{x_d(t)-\epsilon} S(x,t)\, dx = \int_{x_1}^{x_d(t)-\epsilon} \frac{\partial S}{\partial t}\, dx + S(x_d(t)-\epsilon, t)\frac{dx_d(t)}{dt}.$$

Here, the first term will vanish in the limit $x_1 \to x_d(t) - \epsilon$. By collecting terms, substituting back into (8.55), and taking appropriate limits, we obtain what is known as the *Rankine–Hugoniot condition*

$$\sigma(S^+ - S^-) = f(S^+) - f(S^-). \tag{8.56}$$

Here, $S^{\pm}$ denote the saturation values immediately to the left and right of the discontinuity and $\sigma = dx_d/dt$. Equation (8.56) describes a necessary relation between states on opposite

https://doi.org/10.1017/9781108591416.012 Published online by Cambridge University Press

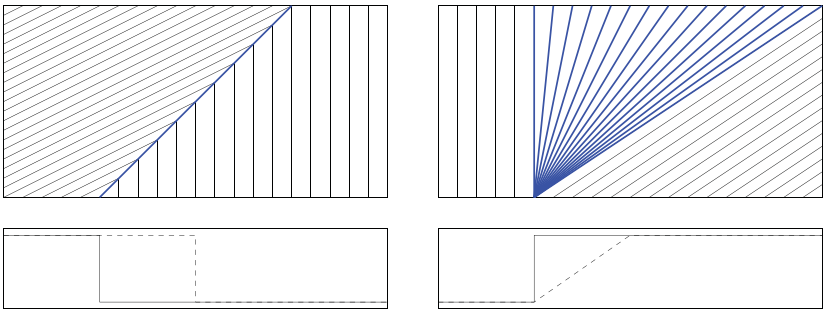

Figure 8.10 Illustration of self-sharpening (left) and spreading waves (right). The upper plots show the characteristics, with the characteristics belonging to the Riemann fan marked in blue. The lower plots show the initial solution (solid line) and the solution after some time (dashed line).

sides of a discontinuity, but does not provide sufficient conditions to guarantee that the resulting discontinuity is physically admissible. To this end, one must use a so-called *entropy condition* to pick out the physically correct solution. If the flux function is strictly convex with $f''(S) > 0$, or strictly concave with $f''(S) < 0$, a sufficient condition is provided by the *Lax entropy condition*,

$$f'(S^-) > \sigma > f'(S^+). \tag{8.57}$$

This condition basically states that the discontinuity must be a *self-sharpening* wave in the sense that saturation values in the interval between S^- and S^+ tend to come closer together upon propagation. Such a wave is commonly referred to as a *shock*, based on an analogy from gas dynamics. In the opposite case of a *spreading wave*, commonly referred to as a *rarefaction wave*, nearby states become more distant upon propagation, and for these continuous waves, the characteristic speeds are increasing in the flow direction. In Figure 8.9 this corresponds to the continuous part of the solution that decays towards the shock. For cases with convex or concave flux function, waves arising from discontinuous initial-boundary data will either be shocks or rarefactions, as illustrated in Figure 8.10. If the flux function is linear, or has linear sections, we can also have linearly degenerate waves for which the characteristic speeds are equal on both sides of the wave.

For cases where the flux function is neither strictly convex nor concave, one must use the more general *Oleinik entropy condition* to single out admissible discontinuities. This condition states that

$$\frac{f(S) - f(S^-)}{S - S^-} > \sigma > \frac{f(S) - f(S^+)}{S - S^+} \tag{8.58}$$

for all values S between S^- and S^+. For the classical displacement case with $S_0 = 0$ and $S_i = 1$, this condition implies that the correct saturation S^* at the shock front is given by

$$f(S^*)/S^* = f'(S^*), \tag{8.59}$$

https://doi.org/10.1017/9781108591416.012 Published online by Cambridge University Press

i.e., the point on the fractional-flow curve at which the chord between the points $(0,0)$ and $(S^*, f(S^*))$ coincides with the tangent at the latter point.

If you are well acquainted with the theory of hyperbolic conservation laws, you will immediately recognize (8.53) as an example of a *Riemann problem*, i.e., a conservation law with a constant left and right state. Let these states be denoted S_L and S_R. If $S_L > S_R$, the solution of the Riemann problem is a self-similar function given by

$$S(x,t) = \begin{cases} S_L, & x/t < f_c'(S_L), \\ \left(f_c'\right)^{-1}(x/t), & f_c'(S_L) < x/t < f_c'(S_R), \\ S_L, & x/t \geq f_c'(S_R), \end{cases} \tag{8.60}$$

which is often referred to as the *Riemann fan*. Here, $f_c(S)$ is the upper concave envelope of f over the interval $[S_R, S_L]$ and $(f_c')^{-1}$ the inverse of its derivative. Intuitively, the concave envelope is constructed by imagining a rubber band attached at S_R and S_L and stretched above f in between these two points. When released, the rubber band assumes the shape of the concave envelope and ensures that $f_c''(S) < 0$ for all $S \in [S_R, S_L]$. The case $S_L < S_R$ is treated symmetrically with f_c denoting the lower convex envelope. The petroleum literature usually attributes this construction to Welge [309]. Figure 8.10 shows examples of two such Riemann fans: a single shock in the left plot and a rarefaction fan in the right plot.

Example 8.4.1 *Let us first consider the Buckley–Leverett solution for a pure imbibition, for which the left and right states are $S_L = 1$ and $S_R = 0$. From the discussion above, we know that the self-similar solution of the associated Riemann problem is found by computing the upper concave envelope of the fraction flux function, which is linear in the interval $[0, S^*]$ and then coincides with $f(S)$ in the interval $[S^*, 1]$, where the saturation S^* behind the shock front is determined from (8.59). If we assume a simple case with relative permeabilities given by the Corey model (8.15) on page 241 with $n_w = n_o = 2$ and $\mu_w/\mu_o = M$, (8.59) reads*

$$\frac{S_M}{S_M^2 + M(1-S_M)^2} = \frac{2M(1-S_M)S_M}{\left(S_M^2 + M(1-S_M)^2\right)^2}.$$

Here, we have used S_M to denote the front saturation $S^* = \sqrt{M/(M+1)}$ to signify that it depends on the viscosity ratio M. Figure 8.11 shows the Buckley–Leverett solution for three different viscosity ratios. In all three cases, the solution consists of a shock followed by a trailing continuous rarefaction wave. When the water viscosity is five times higher than oil ($M = 5$), the mobility of pure oil is five times higher than the mobility of pure water. Hence, we have a favorable *displacement in which the water front acts like a piston that displaces almost all the oil at once. In the opposite case with oil viscosity five times higher than water viscosity, we have an* unfavorable *displacement because the water front is only able to displace a small fraction of the oil. Here, the more mobile oil will tend to finger through the oil and create viscous fingers for displacements in higher spatial dimensions. We will come back to examples that illustrate this later in the book. In the opposite case of*

https://doi.org/10.1017/9781108591416.012 Published online by Cambridge University Press

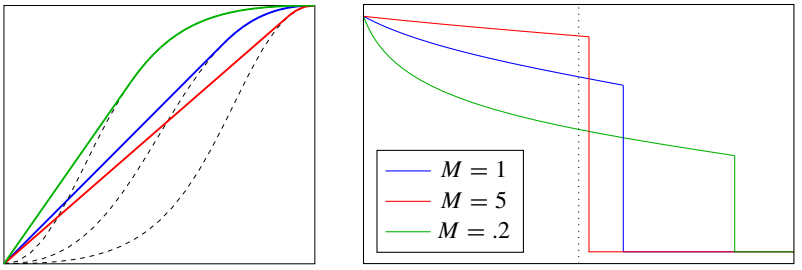

Figure 8.11 Buckley–Leverett solutions for a pure imbibition case with Corey relative permeabilities with exponent $n_w = n_0 = 2$ and mobility ratio $\mu_w/\mu_o = M$. The left plot shows the upper concave envelopes of the flux functions, while the right plot shows the self similar solution $S_w(x/t)$ with $x/t = 1$ shown as a dotted line.

a drainage process, it follows by symmetry that the solution will consist of a shock from 1 *to* $1 - S_M$ *followed by a rarefaction wave from* S_M *to 0.*

Instead of an infinite domain, let us place a producer some distance to the right of the origin. We then see that since the saturation is constant ahead of the shock, the amount of produced oil will be equal the amount of injected water until the first water reaches the producer. This means that the cumulative oil production has a linear slope until water breakthrough. After water has broken through, the well will be producing a mixture of oil and water and the slope of the cumulative oil production decreases.

Let us try to determine the amount of produced oil at water breakthrough. To this end, we can assume that water is injected at $x = 0$ and oil produced at $x = L$. At water breakthrough, the saturation at the producer is $S(x = L) = S^*$. The amount of produced oil equals the amount of water that has displaced it $L\bar{S}$, where $\bar{S}$ is the average water saturation defined as

$$\begin{aligned}\bar{S} &= \frac{1}{L}\int_0^L S\,dx = \frac{1}{L}\Big[xS\Big]_{x=0}^{x=L} - \frac{1}{L}\int_1^{S^*} x\,dS \\ &= S^* - \frac{t}{L}\int_1^{S^*}\Big(\frac{df_c}{dS}\Big)\,dS = S^* - \frac{t}{L}\big[f^* - 1\big].\end{aligned}$$

The second equality follows from the total differential $d(xS) = xdS + Sdx$, while the third equality follows from the equation (8.52) that describes the position $x(t)$ of a constant saturation value at time t. Finally, the water breakthrough occurs at time $t = L/f'(S^*)$, and hence we have that,

$$\frac{1 - f(S^*)}{\bar{S} - S^*} = f'(S^*).$$

We interpret this graphically as follows: S_w is the point at which the straight line used to define the front saturation S^* intersects the line $f = 1$ as shown in Figure 8.12.

https://doi.org/10.1017/9781108591416.012 Published online by Cambridge University Press

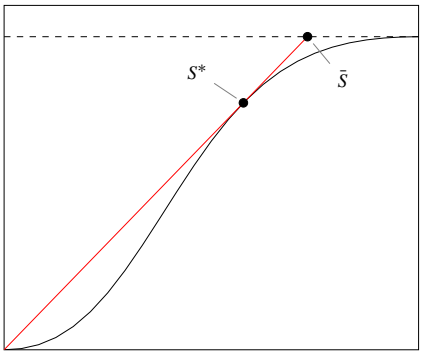

Figure 8.12 Graphical determination of front saturation and average water saturation at water breakthrough.

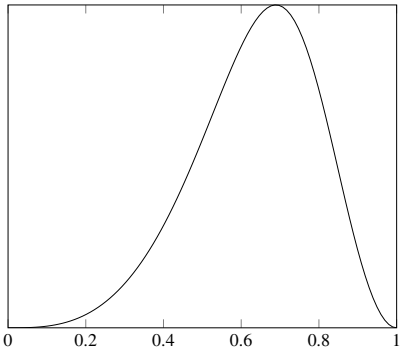

Figure 8.13 Fractional flow function for 1D gravity segregation for Corey relative permeabilities (8.15) with $n_w = 3$, $n_0 = 2$, and mobility ratio $\mu_w = 5\mu_o$ for $\rho_w > \rho_n$.

8.4.2 Gravity Segregation

Next, we consider a pure gravity displacement, for which the transport equation reads,

$$\frac{\partial S}{\partial S} + \frac{\partial}{\partial z}\Big(\frac{\lambda_n \lambda_w}{\lambda_w + \lambda_n}\Big) = 0, \tag{8.61}$$

where we, without lack of generality, have scaled away the constant $g\Delta\rho$. With a slight abuse of notation, we call the flux function for $g(S)$. This flux function will have a characteristic bell-shape, e.g., as shown in Figure 8.13, which points downward if $\rho_w > \rho_n$ and upward in the opposite case. We assume that the wetting fluid is most dense and consider the flow problem with one fluid placed on top of the other so that the fluids are separated by a sharp interface. If the lightest fluid is on top, we have that $S_L < S_R$, and from the discussion of (8.60) on page 262 we recall that the Riemann solution is found by computing the lower convex envelope of $g(S)$. Here, $g_c(S) \equiv 0$ and hence we have a stable situation. In the opposite case, $S_L > S_R$ and $g_c(S)$ is a strictly concave function for

https://doi.org/10.1017/9781108591416.012 Published online by Cambridge University Press

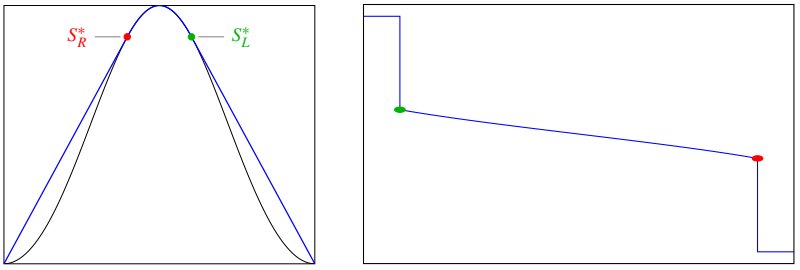

Figure 8.14 Buckley–Leverett solution for a gravity column with sealing top and bottom before the moving fluids have contacted the top/bottom of the domain. (Model: Corey relative permeabilities (8.15) with $n_w == n_0 = 2$, and mobility ratio $\mu_w = \mu_o$ and $\rho_w > \rho_n$.)

which $g_c'(0)' > 0 > g_c'(1)$. This is an unstable situation and the heavier fluid will start to move downward (in the positive z-direction) and the lighter fluid upward (in the negative z-direction) near the interface. Let us consider more details in a specific case:

Example 8.4.2 *We consider a gravity column inside a homogeneous sand body confined by a sealing medium at the top and the bottom. For simplicity, we scale the domain to be* $[0, 1]$, *assume that the initial fluid interface is at* $z = 0.5$, *and use a Corey relative permeability model with* $n_w = n_o = 2$ *and equal viscosities.*

This choice of parameters gives a symmetric flux function $g(S)$, *as shown in the left plot of Figure 8.14. Our initial condition with a heavy fluid on top of a lighter fluid is described by setting* $S_L = 1$ *in the top half of the domain and* $S_R = 0$ *in the bottom half of the domain. As explained above, the Riemann problem is solved by computing the upper concave hull of* $g(S)$. *The hull* $g_c(S)$ *is a linear function lying above* $g(S)$ *between* 0 *and* S_R^*, *follows the graph of* $g(S)$ *in the interval* S_R^* *to* S_L^*, *and is a linear function lying above* $g(S)$ *between* S_L^* *and* 1. *The point* S_R^* *is given by the solution to* $g'(S_R^*)S_R^* = g(S_R^*)$. *At the boundaries* $x = 0, 1$, *we have* $g(S_L) = g(S_R) = 0$, *and hence no-flow conditions as required. Initially, the solution thus consists of three different regions:*

- *a single-phase region on top that only contains the heavier fluid* ($S_L = 1$), *which is bounded above by the lines* $z = 0$ *and below by the position of the shock* $1 \to S_L^*$;
- *a two-phase transition region that consists of a mixture of heavier fluid moving downward and lighter fluid moving upward; this corresponds to a centered rarefaction wave in which the saturation decays smoothly from* S_L^* *to* S_R^*;
- *a single-phase region at the bottom that only contains the light fluid. This region is bounded above by a shock* $S_R^* \to 0$ *and from below* $z = 1$.

As time passes, the two shocks that limit the single-phase regions of heavy and light fluids will move upward and downward, respectively, so that an increasing portion of the fluid column is in a two-phase state; see the right plot in Figure 8.14. Eventually, these shocks will reach the top and bottom of the domain. Because of the symmetry of the problem, it is sufficient for us to only consider one end of the domain, say $z = 0$. *Since we have assumed*

https://doi.org/10.1017/9781108591416.012 Published online by Cambridge University Press

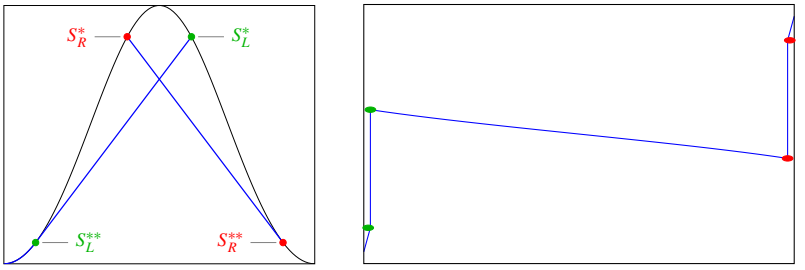

Figure 8.15 Buckley–Leverett solution for a gravity column with sealing top and bottom just after the light/heavy fluids started to accumulate at the top/bottom of the domain. To ensure no-flow, the solution is $S = 0$ at $z = 0$ and $S = 1$ at $z = 1$.

no flow across the top of the domain, the shock $1 \to S_L^*$ *cannot continue to propagate upward. We thus get a Riemann problem, defined by right state* S_L^* *and a left state* S_L*, which could be any value satisfying* $g(S_L) = 0$*. The left state cannot be* 1*, since this would give back the same impermissible shock* $1 \to S_L^*$*. If the left value is* $S_L = 0$ *instead, i.e., a single-phase region with only light fluid forming on the top, the Riemann solution will be given by the concave envelope of* $g(S)$ *over the interval* $[0, S_L^*]$ *and hence will consist fully of waves with positive speed that propagate downward again. The left plot in Figure 8.15 shows the corresponding convex envelope, which we see gives a rarefaction wave* 0 *to* S_L^{**} *and a shock* $S_L^{**} \to S_L^*$*. As the leading shock propagates downward, it will interact with the upward-moving part of the initial rarefaction wave and form a shock, whose right state gradually decays towards* $S = 0.5$*. The solution at the bottom of the domain is symmetric, with accumulation of a single-phase region of the heavy fluid.*

8.4.3 Front Tracking: Semi-Analytical Solutions

Whereas it was quite simple to find an analytical solution in closed form for simple Riemann problems like the ones discussed above, it becomes more complicated for general initial data or when different waves start to interact, as we observed when the two initial shocks reflected from the top and bottom of the gravity column. Generally, one must therefore resort to numerical discretizations in the form of a finite element, difference, or volume method. However, for one-dimensional saturation equations there is a much more powerful alternative, which we will introduce you to very briefly.

In the semi-analytical *front-tracking* method, the key idea is to replace the functions describing initial and boundary values by piecewise constant approximations. For a small time interval, the solution can then be found by piecing together solution of local Riemann problems, and consists of a set of constant states separated by shocks and rarefaction waves. Shocks correspond to the linear parts of the local convex/concave envelopes, whereas rarefaction waves correspond to the nonlinear parts of envelopes. If we further approximate the flux function by a piecewise linear function, all convex/concave envelopes are always

https://doi.org/10.1017/9781108591416.012 Published online by Cambridge University Press

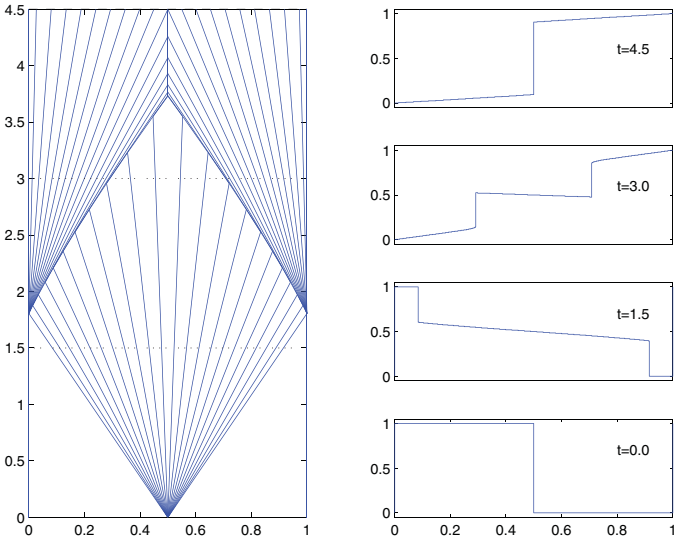

Figure 8.16 Solution for a gravity column with heavy fluid on top of a light fluid computed by front tracking for a model with Corey relative permeabilities with $n_w = n_o = 2$ and equal viscosities. The left column shows the wave pattern in the (z,t) plane, where each blue line corresponds to the propagation of a discontinuous state. The right column shows the solution $S(z,t)$ at four different times.

piecewise linear, and the solution of Riemann problems will consist only of shocks. In other words, the solution to the continuous, but approximate PDE problem consists entirely of constant states separated by discontinuities propagating at a constant speed given by the Rankine–Hugoniot condition (8.56) on page 260.

Each time two or more discontinuities "collide," we have a new Riemann problem that gives rise to a new set of discontinuities emanating out of the collision point. Computing local convex/concave envelopes and keeping track of propagating discontinuities can be formulated as numerical algorithms, and we end up with a semi-analytical method, which is unconditionally stable and formally first-order accurate. In fact, one can prove that for any finite spatial domain, there will be a finite number of shock collisions, and hence we can compute an approximate solution up to infinite time in a finite number of steps; see [134] for more details. In the following example, we use this method to study a few simple 1D cases.

Example 8.4.3 *We continue to study gravity segregation of a heavy fluid placed on top of a lighter fluid inside a sand box with sealing top and bottom. Figure 8.16 shows the solution computed by approximating the flux function with a piecewise linear function with 100 equally spaced segments. Initially, the solution contains two constant states* $S_L = 1$ *and* $S_R = 0$*, separated by a composite wave that consists of an upward-moving shock, a centered rarefaction wave, and a downward moving shock, as explained earlier*

https://doi.org/10.1017/9781108591416.012 Published online by Cambridge University Press

in Example 8.4.2. Notice that the approximate solution at time $t = 1.5$ is of the same form as shown in Figure 8.14, except that in the approximate front-tracking solution, the continuous rarefaction wave is replaced by a sequence of small discontinuities.

The right plot in Figure 8.15 illustrated the form of the exact solution just after the two initial shocks have reflected at the top and bottom of the domain. Figure 8.16 shows the solution after the reflected waves have propagated some time upward/downward. Here, we clearly see that these waves consist of a fast shock wave followed by a rarefaction wave. As the leading shock interacts with the centered rarefaction wave originating from $(0.5, 0)$, the difference between left and right states diminishes, and the shock speeds decay. Later, the two shocks collide and form a stationary discontinuity that will eventually become a stable steady state with the lighter fluid on top and the heavier fluid beneath.

In general, the transport in an inclined reservoir section will be driven by a combination of gravity segregation and viscous forces coming from pressure differentials. The next example studies one such case.

Example 8.4.4 (CO_2 storage) *We consider two highly idealized models of CO_2 storage in an inclined aquifer with a slow drift of brine either in the upslope or in the downslope direction. If the injection point lies deeper than approximately 800 meters below the sea level, CO_2 will appear in the aquifer as a supercritical liquid phase having much lower density than the resident brine. The injected fluid, which is commonly referred to as the CO_2 plume, will therefore tend to migrate in the upslope direction. As our initial condition, we assume (somewhat unrealistically) that CO_2 has been injected so that it completely fills a small section of the aquifer $x \in [\frac{1}{4}, \frac{3}{4}]$. To study the migration after injection has ceased, we can now use a fractional flow function of the form,*

$$F(S) = \frac{S^2 \mp 4S^2(1-S)^3}{S^2 + \frac{1}{5}(1-S)^3},$$

where the minus sign denotes upslope background drift and the plus sign downslope drift. Figure 8.17 shows the flux functions along with the envelopes corresponding to the two Riemann problems.

Let us first consider the case with upslope drift. At the tip of the plume ($x = \frac{3}{4}$), there will be a drainage process in which the more buoyant CO_2 displaces the resident brine. This gives a composite wave that consists of a shock $S_d^* \to 1$ that propagates upslope, followed by a centered rarefaction wave from S_d^* to S_d^{**} having wave speeds both upslope and downslope. The rarefaction is followed by a trailing shock wave $0 \to S_d^{**}$ that propagates in the downslope direction. Likewise, at the trailing edge of the plume, the resident brine will imbibe into CO_2, giving a wave consisting of a shock $S_i^* \to 0$ followed by a rarefaction wave, both propagating in the upslope direction. The two Riemann fans can be seen clearly in Figure 8.18, and will stay separated until $t \approx 0.18$, when the shock from the imbibition process collides with the trailing drainage shock. The result of this wave interaction is a new and slightly weaker shock that propagates increasingly faster in the upslope direction,

https://doi.org/10.1017/9781108591416.012 Published online by Cambridge University Press

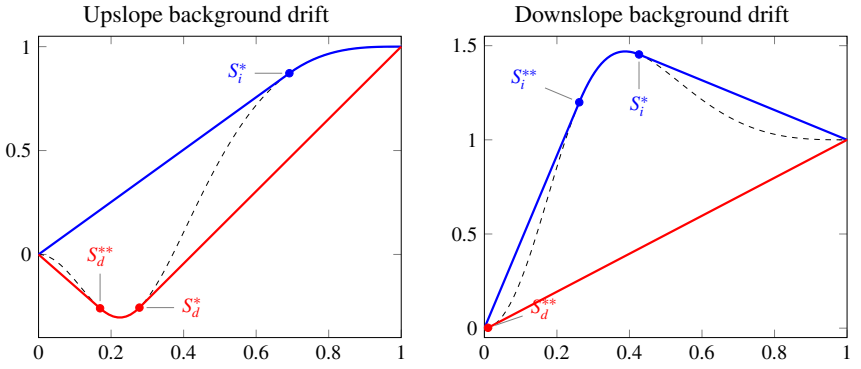

Figure 8.17 Flux functions for the CO_2 migration example. The dashed curves are the flux function $F(S)$, which accounts for a combination of gravity segregation and viscous background drift. The blue lines show the concave envelopes corresponding to imbibition at the left edge of the plume, while the red lines are the convex envelopes corresponding to drainage at the right edge the plume.

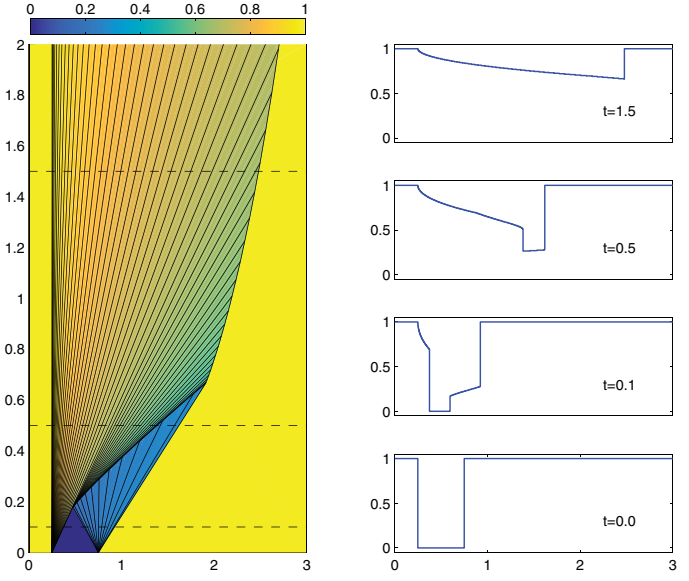

Figure 8.18 Solution for a conceptual model of CO_2 injected into an inclined 1D aquifer with a background upslope drift. Upslope direction is to the right. Dashed lines in the left plot signify the snapshots shown in the right column.

followed by a continuous rarefaction wave, which is an extension of the initial imbibition rarefaction. At time $t \approx 0.665$*, the new shock wave has overtaken the tip of the plume, and the result of this interaction is that the upslope migration of the plume gradually slows down.*

https://doi.org/10.1017/9781108591416.012 Published online by Cambridge University Press

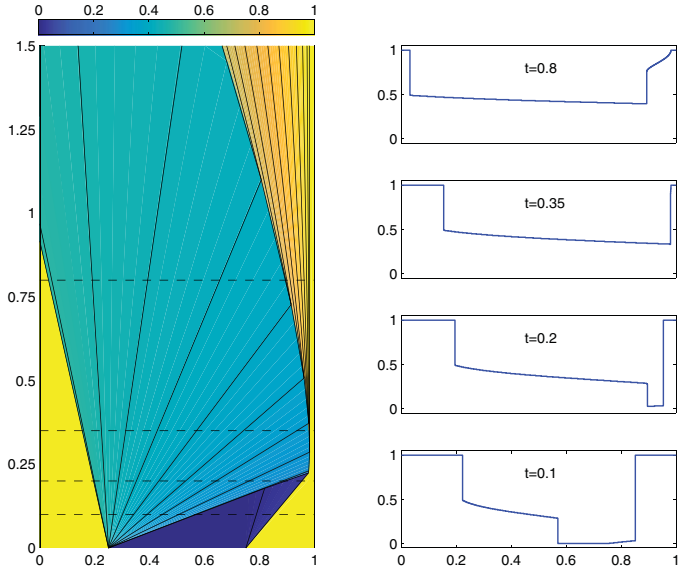

Figure 8.19 Solution for a conceptual model of CO_2 injected into an inclined 1D aquifer with a background downslope drift. Upslope direction is to the left.

If we remove the upslope drift, the initial imbibition process is no longer present, but the long-term behavior remains the same and consists of a leading shock wave followed by a rarefaction that slowly eats up and slows down the shock.

Figure 8.19 shows the opposite case with a downslope background drift. Here, the imbibition process at the left edge of the plume gives a shock $0 \rightarrow S_i^{**}$ *that propagates in the downslope direction (to the right in the figure), a centered rarefaction wave from* S_i^{**} *to* S_i^* *with waves that propagate both in the downslope and upslope direction, followed by a shock* $S_i^* \rightarrow 1$ *that propagates upslope. The drainage at the right edge gives a strong shock* $S_d^* \rightarrow 1$ *that propagates downslope, followed by a weak rarefaction wave from* 0 *to* S_d^**. At time* $t \approx 0.25$ *the downslope imbibition shock has overtaken both the rarefaction wave and the shock from the drainage process. The resulting wave interaction first forms a stationary shock with left state* S_i^{**}*. However, as the positive part of the imbibition rarefaction wave continues to propagate downslope, the left state gradually increases, and at some point the left state passes the value* $S = \sqrt{1/10}$ *for which* $F(S) = 1$*. When this happens, the stationary shock turns into a composite wave consisting of a shock and a trailing rarefaction wave that both propagate in the upslope direction.*

Figure 8.20 shows the two migration cases over a longer time. Injecting CO_2 *so that it must migrate upward against a downslope brine drift is clearly advantageous since it will delay the upslope migration of the gradually thinning plume.*

The purpose of the previous example was to introduce you to the type of wave patterns that arise in hyperbolic saturation equations, and show that these can be relatively complicated even for simple initial configurations. While front-tracking is probably the best method

https://doi.org/10.1017/9781108591416.012 Published online by Cambridge University Press

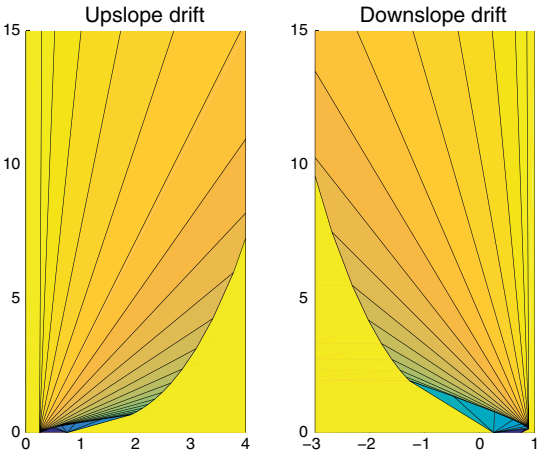

Figure 8.20 Long-time solutions for the two conceptual models of CO_2 storage.

you can find to study wave patterns in 1D hyperbolic saturation equations, it would not be the method of choice to study multiphase flow models in multiple spatial dimensions, unless we use a streamline method that transform the 3D transport problems to a family of 1D problems. In the next chapter, we therefore continue to discuss finite-volume methods that are more suitable for multidimensional reservoir simulation. In simulation of real reservoirs, one cannot hope to resolve the dynamics to the level of detail seen in the last example. To be able to compute shocks and other types of discontinuities, finite-volume (and finite-element) methods contain a certain amount of numerical dissipation that tends to smear any discontinuity. Likewise, strong heterogeneities and radial flow near wells can introduce orders of magnitude variations in Darcy velocities. This necessitates the use of small time steps or implicit temporal discretizations, which both tend to smear discontinuities and make it more difficult to resolve complex wave interactions in full detail.

We end our discussion of 1D solutions with a few remarks about the simulation of CO_2 storage, since this was touched upon conceptually in Example 8.4.4. In more realistic modeling of CO_2 storage, one would need a more detailed model that accounts for the effect that the lighter CO_2 plume will flow to the top of the formation and migrate upslope as a thin layer under the sealing caprock that bounds the aquifer from above. This can be done by either using a 3D or a 2D cross-sectional saturation equation, possibly coupled with a pressure equation. However, the most efficient approach to study large-scale, long-term CO_2 migration is to integrate the pertinent flow equations in the vertical direction to form a vertically averaged model that accounts for the vertical fluid distribution in an averaged sense. MRST has a large module, `co2lab`, that offers a wide variety of vertically averaged models and other types of reduced models suitable for modeling of large-scale CO_2 storage. A discussion of such models is beyond the scope of this book. I you are interested in more details, you should instead consult one of the papers describing the methods implemented in `MRST-co2lab` [19, 230, 227, 228, 232, 193, 21].

https://doi.org/10.1017/9781108591416.012 Published online by Cambridge University Press